Study of reactions $\pi^+p \to (\rho^0,\omega)\Delta^{++}(1236)$ at 10.3 GeV/c

J. Beaufays, C. N. Kennedy,* A. W. Key, J. D. Prentice, and P. D. Zemany†
Department of Physics, University of Toronto, Toronto, Ontario M5S 1A7, Canada
(Received 27 December 1977)

Cross sections, differential cross sections, single and joint spin-density matrix elements are given for the reactions $\pi^+p \to (\rho^0,\omega)\Delta^{++}$ at 10.3 GeV/c. Correlations between the vector-meson and the Δ^{++} decay angular distributions are observed. A discussion of the results in terms of particle exchange, SU(3) symmetry, quark additivity, and the equal-phase hypothesis is presented. The amplitudes for the process $\pi^+p \to \rho^0\Delta^{++}$ are extracted by a model-dependent analysis and compared with current theoretical predictions.

I. INTRODUCTION

The study of two-body reactions with unstable particles in the final states provides detailed information on the production mechanism, although the number of measurable quantities in general does not allow a complete amplitude analysis.

Here we study the reactions

$$\pi^+p \to \rho^0\Delta^{++}(1236) \tag{1}$$

and

$$\pi^+p \to \omega\Delta^{++}(1236) \tag{2}$$

at an incident pion momentum of 10.3 GeV/c. Many studies of these reactions in the energy range from 2 to 18 GeV/c have been reported.[1,2]

In Regge phenomenology, there are many advantages to studying the quasi-two-body reactions (1) and (2): The presence of Δ^{++} in the final state, and G-parity conservation, introduce additional constraints on the quantum numbers of the exchange trajectories. However, it is known that Regge-pole exchange is not the only contribution to the amplitudes and that corrections to simple exchange are needed to describe the data. We shall use the word "cut," as usual, to denote this non-pole-like part of an amplitude, which might be related to a cut in the complex l plane, and which may arise, for example, from absorptive corrections. These cut effects, which from the present theoretical point of view should be largest in the zero-helicity-flip amplitudes, may tend to mask the supposed Regge nature of the amplitudes and obscure some of their properties, such as factorization or SU(3) symmetry. Therefore an experimental investigation of the deviation of these properties from the predictions of a pure Regge model can provide information on the size and the nature of these cut contributions. In addition, tests of the theoretical predictions of, for example, the naive quark model may give information on the relative importance of the amplitudes and aid in the understanding of the production mechanism.

This paper is organized as follows. In Sec. II, the data for reactions (1) and (2) are presented. The determination of cross sections, differential cross sections, single spin-density matrix elements, joint spin-density matrix elements, and joint decay correlations is presented in Sections III, IV, V, and VI, respectively. In Sec. VII, the contributions of natural- and unnatural-spin-parity exchanges are investigated. A discussion of the polarization properties of the vector meson is given in Sec. VIII. In Sec. IX, the question of whether or not all helicity amplitudes have the same phase is investigated by a model-independent method for reaction (1). In Secs. X, XI, and XII, our data are compared with the predictions of different theoretical models: factorization, SU(3), and quark additivity respectively. Finally, in Sec. XIII, the results of an amplitude analysis are presented for reaction (1).

II. THE DATA

The data were obtained from a 300 000-picture exposure of the SLAC 82-in. hydrogen-filled bubble chamber to a π^+ beam of central momentum 10.3 GeV/c. Using event-selection criteria described in Ref. 3, we have obtained the following numbers of events in the final states of interest:

$$\pi^+p \to p\pi^+\pi^+\pi^- \quad 9\,983 \text{ events}, \tag{3}$$

$$\pi^+p \to p\pi^+\pi^+\pi^-\pi^0 \quad 10\,428 \text{ events}. \tag{4}$$

After appropriate corrections these reactions correspond to experiments of (6.18 ± 0.44) events/μb and (5.50 ± 0.39) events/μb, respectively.

III. CROSS SECTIONS

A. $\pi^+p \to \rho^0\Delta^{++}(1236)$

The number of $\rho^0\Delta^{++}$ events in reaction (3) was extracted using the slice technique of Aguilar-Benitez *et al.*[4] We first define $-t(p \to \Delta)$, the negative of the square of the four-momentum transfer from the target proton to the outgoing $(p\pi^+)$

system, and remove events with $-t(p \to \Delta) > 1.0$ GeV^2. The $(p\pi^+)$ invariant-mass spectrum is then divided into ten slices between

$$1.07 \leq m(p\pi^+) \leq 1.70 \text{ GeV}. \quad (5)$$

For each slice, the number of ρ^0 events was determined by a minimum χ^2 fit to the corresponding $(\pi^+\pi^-)$ invariant mass spectrum in the region

$$0.4 \leq m(\pi^+\pi^-) \leq 0.9 \text{ GeV}. \quad (6)$$

The functional form used in each fit was a P-wave Breit-Wigner function multiplied by phase space and a second-order polynomial in mass. The Breit-Wigner function used a central mass of $m_\rho = 771 \pm 3$ MeV and a width of $\Gamma_\rho = 157 \pm 9$ MeV, values obtained from a fit to the combined $(\pi^+\pi^-)$ mass spectrum of all ten slices using the same parametrization as above. The resultant distribution of the number of ρ^0 events plotted as a function of $(p\pi^+)$ invariant mass, displayed in Fig. 1, shows a large Δ^{++} signal over a small background. This distribution was then fitted to a P-wave Breit-Wigner function multiplied by phase space and a polynomial background to yield the number of $\rho^0\Delta^{++}$ events in the fitted region. This number was then corrected by the ratio of the number of ρ^0 events calculated to lie within four resonance widths Γ^0 of the central mass m_ρ to the number of events in the mass region defined in Eq. (6), a factor of 1.18. The resulting number of events is 2511 ± 55 in the mass regions defined by

$$1.07 \leq M(p\pi^+) \leq 1.70 \text{ GeV},$$

$$m_\rho - 4\Gamma_\rho \leq m(\pi^+\pi^-) \leq m_\rho + 4\Gamma_\rho.$$

This corresponds to a cross section, with statistical error, of

$$\sigma(\pi^+ p \to \rho^0\Delta^{++}(1236)) = 406 \pm 12 \ \mu\text{b}. \quad (7)$$

The energy dependence of $\sigma(\pi^+ p \to \rho^0\Delta^{++}(1236))$ is shown in Fig. 2.[1] The functional form

$$\sigma \propto p_{\text{lab}}{}^{-n} \quad (8)$$

gives a poor fit to the data with $p_{\text{lab}} \geq 4.0$ GeV/c (χ^2 probability $<10^{-4}$) and a value of $n = 1.25 \pm 0.04$. The large χ^2, however, appears to arise more from normalization errors between different experiments than from a systematic deviation from this fit.

B. $\pi^+ p \to \omega\Delta^{++}(1236)$

The number of $\omega\Delta^{++}$ events in reaction (4) was also extracted using the slice technique. The $(\pi^+\pi^-\pi^0)$ mass spectrum for events with $-t(p \to \Delta) < 1.0$ GeV^2 was divided into ten slices between

$$0.60 \leq m(\pi^+\pi^-\pi^0) \leq 0.96 \text{ GeV}. \quad (9)$$

The region defined by Eq. (9) includes all events

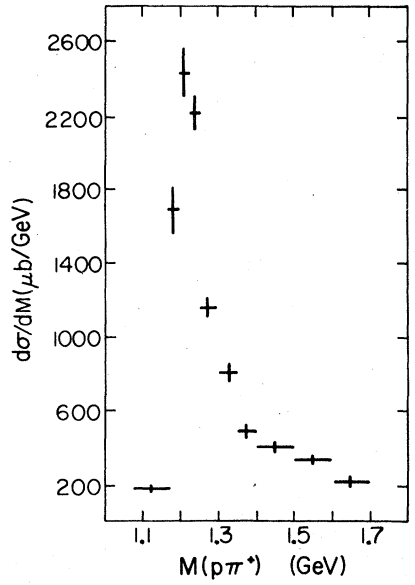

FIG. 1. Number of ρ^0 events, plotted as a function of the $p\pi^+$ invariant mass, from the reaction $\pi^+ p \to p\pi^+\pi^+\pi^-$.

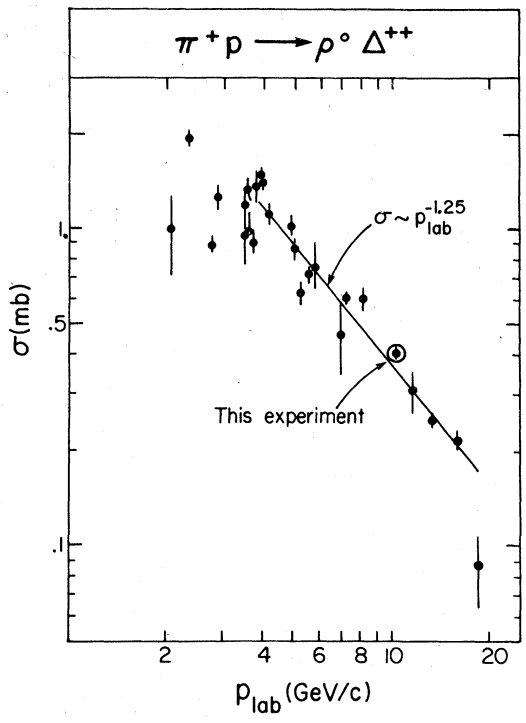

FIG. 2. Cross sections for the reaction $\pi^+ p \to \rho^0\Delta^{++}(1236)$ as functions of p_{lab}. The straight line represents the fit with the expression $\sigma \propto p_{\text{lab}}{}^{-n}$.

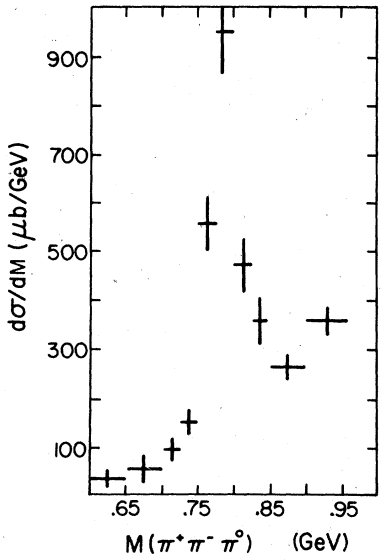

FIG. 3. Number of $\Delta^{++}(1236)$ events, plotted as functions of the $\pi^+\pi^-\pi^0$ invariant mass, from the reaction $\pi^+ p \to p\pi^+\pi^+\pi^-\pi^0$.

within four effective resonance widths ($\Gamma_\omega^{\text{eff}} = 47 \pm 5$ MeV) of a central mass value ($m_\omega = 787 \pm 4$ MeV). m_ω and $\Gamma_\omega^{\text{eff}}$ were determined by a fit of the overall $(\pi^+\pi^-\pi^0)$ mass spectrum, for events which satisfied the $-t$ cut and Eq. (5), to a P-wave Breit-Wigner function added to a second-order polynomial. For each slice, a maximum-likelihood fit to the corresponding $(p\pi^+)$ mass spectrum defined by Eq. (5) was performed. This fit used a matrix element with a Breit-Wigner function [with fixed parameters $m_\Delta = 1246 \pm 6$ MeV and $\Gamma_\Delta = 146 \pm 28$ MeV, determined from an overall fit to all events satisfying Eqs. (5) and (9)] multiplied by phase space and a polynomial background. The number of Δ^{++} events, so obtained, in each $(\pi^+\pi^-\pi^0)$ mass slice is shown in Fig. 3. To account for the experimental mass resolution in the ω region the resonance shape of Fig. 3 is now described by the folding integral[5]

$$F(m) = \int dx\, F_{\text{BW}}(x) r(|x - m|),$$

where F_{BW} stands for a P-wave Breit-Wigner shape and r for a Gaussian resolution function with standard deviation 9 MeV. The background was described by a polynomial shape added incoherently. This last parametrization gives the values of the central mass, $m_\omega = 787 \pm 4$ MeV, and of the width, $\Gamma_\omega = 14 \pm 5$ MeV, for the ω resonance. The fit yields 304 ± 17 $\omega\Delta^{++}$ events satisfying $-t < 1.0$ GeV^2 in the mass region defined by Eqs. (5) and (9), which corresponds, after correction for

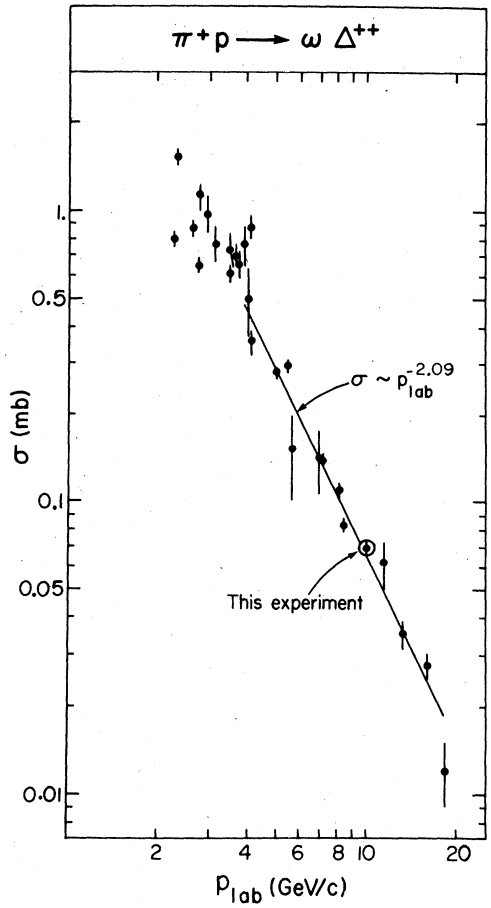

FIG. 4. Cross sections for the reaction $\pi^+ p \to \omega\Delta^{++}(1236)$ as functions of p_{lab}. The straight line represents the fit with the expression $\sigma \propto p_{\text{lab}}^{-n}$.

the neutral/charged branching ratio of the ω, to a cross section, with statistical error, of

$$\sigma(\pi^+ p \to \omega\Delta^{++}(1236)) = 69 \pm 4\ \mu\text{b}. \qquad (10)$$

The energy dependence of $\sigma(\pi^+ p \to \omega\Delta^{++}(1236))$ is shown in Fig. 4.[2] A fit to the data having $p_{\text{lab}} \geq 4$ GeV/c, with the power law (8), again yields a poor fit with $n = 2.09 \pm 0.05$ which is shown by the line in Fig. 4. Again the fitted line appears to represent the data well and the large χ^2 is probably due to relative normalization errors between experiments.

IV. DIFFERENTIAL CROSS SECTIONS

As our statistics are not sufficient to allow us to use the slice technique as a function of momentum transfer, we used the traditional method of taking events in the $\rho^0\Delta^{++}$ $(\omega\Delta^{++})$ overlap region to extract the differential cross sections.

TABLE I. Differential cross section $d\sigma/dt$ for the reaction $\pi^+p \to \rho^0\Delta^{++}(1236)$.

$-t$ (GeV^2)	No of events [a]	No. of background events [a]	$d\sigma/dt$ (mb/GeV^2)
0.03–0.04		(302)	5886 ± 381
0.04–0.05		(287)	4643 ± 274
0.05–0.06	155	21	4239 ± 261
0.06–0.08	224	32	2839 ± 151
0.08–0.10	144	24	1723 ± 118
0.10–0.12	129	26	1488 ± 109
0.12–0.14	94	17	1132 ± 95
0.14–0.16	78	9	1011 ± 90
0.16–0.18	53	11	574 ± 68
0.18–0.20	41	8	436 ± 59
0.20–0.25	84	22	404 ± 36
0.25–0.30	55	9	236 ± 28
0.30–0.35	47	12	229 ± 27
0.35–0.40	34	6	197 ± 25
0.40–0.50	46	9	118 ± 13
0.50–0.70	55	8	67 ± 7
0.70–1.00	31	12	16 ± 3

[a] For the corrected bins (see text) only the number of normalized background-subtracted events is given.

A. $\pi^+p \to \rho^0\Delta^{++}(1236)$

The number of events in the $\rho^0\Delta^{++}$ overlap region defined by

$$\text{region } \alpha \begin{cases} \rho^0\text{: } 0.62 \leq m(\pi^+\pi^-) \leq 0.92 \text{ GeV}, \\ \Delta^{++}\text{: } 1.14 \leq m(p\pi^+) \leq 1.34 \text{ GeV} \end{cases} \quad (11)$$

is given in Table I as a function of $-t$.

For the small percentage of events for which more than one combination lay in this interval, the combination with the smallest $-t$ was chosen as the $\rho^0\Delta^{++}$ event.

In region α there are three processes which represent background to reaction (1):

$$\pi^+p \to \rho^0\pi^+p\,, \quad (12)$$

$$\pi^+p \to \pi^+\pi^-\Delta^{++}\,, \quad (13)$$

$$\pi^+p \to \pi^+\pi^-\pi^+p\,. \quad (14)$$

An investigation of the $\rho^0\pi^+ - \pi^+p$ Dalitz plot reveals that the dominant components of (12) are the final states

$$\pi^+p \to A_1^+p \searrow \rho^0\pi^+$$

and

$$\pi^+p \to A_3^+p \searrow \rho^0\pi^+\,,$$

where A_1 and A_3 are the broad low-mass 3π enhancements. Similarly, the $N^*(1470)$ and $N^*(1700)$ isobars dominate the final state (14). Since the relevant Dalitz plots indicate that all these enhancements contribute less than 5% background to reaction (1), no attempt has been made to remove this contamination.

The remaining background $-t$ distribution from reactions (13) and (14) was simply estimated from the sidebands of the ρ^0:

$$0.48 \leq m(\pi^+\pi^-) \leq 0.58 \text{ GeV}\,,$$

$$0.96 \leq m(\pi^+\pi^-) \leq 1.06 \text{ GeV}\,.$$

This background, which is essentially due to the $\pi^+\pi^-$ S wave, is found to have the same $-t$ dependence as that of region α. This procedure, while it overestimates the amount of background by including the contribution from the tails of the ρ^0, has thus no effect on the shape of the extracted distribution. The number of events comprising the estimated background from reactions (13) and (14) is given as a function of $-t$ in Table I.

We define $-t_{\min}$ as the minimum kinematically allowed value of $-t(p \to \Delta)$, and $t' = |t - t_{\min}|$. The value of $-t_{\min}$ is a function of the domain chosen to define the ρ^0 and Δ^{++} resonances; in particular, the limits of region α have different values of $-t_{\min}$ which we define by $-t_{\min}^{\min}(\alpha)$ (= 0.008 GeV^2) and $-t_{\min}^{\max}(\alpha)$ (= 0.044 GeV^2). The quoted cross section in the region between $-t_{\min}^{\min}(\alpha)$ and $-t_{\min}^{\max}(\alpha)$ is thus biased by this purely kinematic constraint. To obtain an unbiased distribution between these values, a smaller slice of region α, defined by

$$\text{region } \beta \begin{cases} 0.62 \leq m(\pi^+\pi^-) \leq 0.77 \text{ GeV}, \\ 1.14 \leq m(\pi^+p) \leq 1.24 \text{ GeV}, \end{cases}$$

was used and a background subtraction on the events in this region was performed as described above. The resulting $-t$ distribution extends unbiased to a lower value of $-t$ [$-t_{\min}^{\max}(\beta) = 0.021$ GeV^2] than the corresponding distribution in region α. The distribution in area β between $-t_{\min}^{\max}(\alpha)$ and $-t_{\min}^{\max}(\beta)$ was then normalized to area α by multiplying by the ratio of the number of background subtracted events with $-t$ values greater than $-t_{\min}^{\max}(\alpha)$ in region α to that in the corresponding sample in region β. The resultant corrected numbers of events are given in parentheses in Table I, along with the corrected $d\sigma/dt$ distribution, after background subtractions and normalization to the total cross section of Eq. (7).

A fit to the differential cross section $d\sigma/dt'$ for $t' < 0.6$ GeV^2 to a sum of two exponentials

$$d\sigma/dt' = A\exp(-C_1t') + B\exp(-C_2t')$$

yields $C_1 = (29.2 \pm 0.9)$ GeV^{-2}, $C_2 = (5.6 \pm 0.1)$ GeV^{-2}, and $A/B = 5.9$ [$\chi^2/\text{NDF} = \frac{11}{9}$, $P(\chi^2) = 28\%$]. These values of this slope are similar within errors to

those obtained at 11.7,[1u] 13.1,[1v] and 16.0[1w] GeV/c, although less than those obtained at lower energies.[1a-1t] However, as noted by Wolf,[6] this shrinkage may be caused entirely by kinematical effects [due, for example, to the nonzero widths of the ρ^0 and $\Delta^{++}(1236)$].

B. $\pi^+ p \to \omega\Delta^{++}(1236)$

A method similar to that described above was used to extract the $\omega\Delta^{++}(1236)$ differential cross section in the overlap region defined by

$$\text{region } \gamma \begin{cases} \omega\text{: } 0.74 \leq m(\pi^+\pi^-\pi^0) \leq 0.82 \text{ GeV}, \\ \Delta^{++}\text{: } 1.14 \leq m(p\pi^+) \leq 1.34 \text{ GeV}. \end{cases} \tag{15}$$

To ensure that these data have a symmetric missing-mass-squared (MM^2) distribution around $m_{\pi^0}{}^2$, the following cut was imposed:

$$|MM^2 - m_{\pi^0}{}^2| \leq 2m_{\pi^0}{}^2 .$$

When more than one combination lay in region γ, the combination with the smallest $-t$ was chosen as the $\omega\Delta^{++}$ event. The number of events in region γ is given as a function of $-t$ in Table II.

Three processes which contribute background to reaction (2) are

$$\pi^+ p \to \omega\pi^+ p , \tag{16}$$

$$\pi^+ p \to \pi^+\pi^-\pi^0\Delta^{++} , \tag{17}$$

$$\pi^+ p \to \pi^+\pi^-\pi^0 p\pi^+ . \tag{18}$$

The dominant contribution to (16) is from the final state

$$\pi^+ p \to B^+ p \quad , \qquad B^+ \to \omega\pi^+$$

where we define B^+ by $m(\omega\pi^+) \leq 1.35$ GeV. Parity conservation implies that the B decay is symmetric in $\cos\theta_B$, where θ_B is the helicity angle between the B direction defined in the overall center of mass and the outgoing ω in the B rest frame. At this energy, events with $\cos\theta_B < 0$ are kinematically inhibited from having a value of $m(p\pi^+)$ in region γ. For events in the B region with $\cos\theta_B < 0$, we invert the ω and the π^+ directions in the B rest frame; if the value of $m(p\pi^+)$ for this new event then lies in region γ we consider it as an example of the parity reflection which contributes to the background of region γ. The new $-t$ for such an inverted event is calculated and subtracted from the distribution of region γ.

The background $-t$ distribution from reactions (17) and (18) was estimated from the sidebands of the ω:

$$0.66 \leq m(\pi^+\pi^-\pi^0) \leq 0.70 ,$$

$$0.86 \leq m(\pi^+\pi^-\pi^0) \leq 0.90 \text{ GeV} .$$

The events comprising the total estimated background from reactions (16)–(18) are given as a function of $-t$ in Table II, along with the resultant $d\sigma/dt$ distribution, after background subtractions and normalization to the total cross section of Eq. (10).

A fit to the differential cross section, $d\sigma/dt'$, for $t' < 0.6$ GeV^2 to the expression

$$d\sigma/dt' = Bt' e^{-At'}$$

yields $A = 8.55 \pm 0.28$ GeV^{-2} [$\chi^2/\text{NDF} = \frac{6}{8}$, $P(\chi^2) = 53\%$]. Comparison of these values to those obtained at other energies[2] reveals an increase of the slope of $d\sigma/dt'$ with increasing energy.

TABLE II. Differential cross section $d\sigma/dt$ for the reaction $\pi^+ p \to \omega\Delta^{++}(1236)$.

$-t$ (GeV^2)	No. of events	No. of background events	$d\sigma/dt$ (μb/GeV^2)
0.02–0.06	17	4	95 ± 20
0.06–0.10	23	9	123 ± 24
0.10–0.15	31	7	171 ± 25
0.15–0.20	33	7	185 ± 26
0.20–0.25	27	5	156 ± 24
0.25–0.30	18	2	112 ± 20
0.30–0.40	30	5	85 ± 12
0.40–0.60	30	6	42 ± 8
0.60–1.10	15	2	12 ± 2

V. SINGLE SPIN-DENSITY MATRIX ELEMENTS

More detailed information on the production mechanism of reactions (1) and (2) can be obtained from the study of the single spin-density matrix elements of the vector-meson and $\Delta^{++}(1236)$ resonances. These elements were determined in the Gottfried-Jackson and helicity frames. In the Gottfried-Jackson frame, the quantization (z) axis points along the direction of the incoming particle (beam for ρ^0 or ω decay and target for Δ^{++} decay) as seen in the rest frame of the decaying resonance. In the helicity frame, the z axis lies along the direction of motion of the decaying system. In both cases, the y axis is chosen as the direction of the normal to the production plane, while x axes are chosen so that the coordinate systems are right-handed. The polarization analyzers were chosen as the decay π^+ for $\rho^0 \to \pi^+\pi^-$ decay, the decay proton for $\Delta^{++} \to p\pi^+$ decay, and the normal to the decay plane for $\omega \to \pi^+\pi^-\pi^0$ decay.

The general formalism allowing the extraction of the 1^- and $\frac{3}{2}^+$ single spin-density matrix elements corrected for the influence of S-wave back-

ground underneath the resonances has been given by Lohmann and Schreiber.[7]

A. $\pi^+ p \to \rho^0 \Delta^{++}(1236)$

As emphasized by these authors, the ρ^0 spin-density matrix elements cannot be determined from the decay angular distribution alone. However, starting with the hypothesis that an S and a P wave, and a P wave, respectively, are necessary to describe the $(\pi^+\pi^-)$ and the $(p\pi^+)$ mass spectra in region α, the differential cross section $d\sigma/dm_{\pi\pi}d\Omega_\rho$, where $\Omega_\rho = (\theta_\rho, \phi_\rho)$ are the usual Gottfried-Jackson or helicity angles of the meson, may be written[8]

$$\frac{d\sigma}{dm_{\pi\pi}d\Omega_\rho} = \epsilon_S |M_S|^2 + (1-\epsilon_S)|M_P|^2 \overline{W}(\cos\theta_\rho, \phi_\rho) . \tag{19}$$

$\overline{W}(\cos\theta_\rho, \phi_\rho)$ is the symmetrized angular distribution, $\overline{W}(\cos\theta_\rho, \phi_\rho) = \frac{1}{2}[W(\cos\theta_\rho, \phi_\rho) + W(-\cos\theta_\rho, \pi - \phi_\rho)]$, where $W(\cos\theta_\rho, \phi_\rho)$ is the angular distribution corresponding to the decay of a 1^- particle. M_S and M_P represent the mass-dependent part of the S and P partial-wave amplitudes, normalized according to

$$\int_{m_1}^{m_2} |M_i|^2 dm_{\pi\pi} = \sigma ,$$

where m_1 and m_2 are the limits of the $(\pi^+\pi^-)$ mass interval considered. Equation (19), integrated over the angular vairables (θ_ρ, ϕ_ρ), yields

$$\frac{d\sigma}{dm_{\pi\pi}} = \epsilon_S |M_S|^2 + (1-\epsilon_S)|M_P|^2 .$$

Maximum-likelihood fits of this function to the $(\pi^+\pi^-)$ mass spectrum of region α yielded ϵ_S, the amount of S-wave background in each $-t$ interval. For $|M_P|^2$ we used the P-wave Breit-Wigner function, while $|M_S|^2$ was represented by a second-order polynomial in mass. The method of moments yields the following functions of ϵ_S and the pure ρ^0 density matrix elements ρ^{00}, ρ^{1-1}, and Re ρ^{10}:

$$\rho^{00} = \tfrac{1}{3}[\epsilon_S + \tfrac{1}{2}(15\langle\cos^2\theta\rangle - 5)] ,$$

$$\rho^{1-1} = -\tfrac{5}{4}\langle\sin^2\theta\cos 2\phi\rangle ,$$

$$\text{Re } \rho^{10} = \frac{5}{2\sqrt{2}}\langle\sin\theta\cos\theta\cos\phi\rangle .$$

The resultant values of the density matrix elements, renormalized to fulfill the P-wave trace condition, $2\rho^{11} + \rho^{00} = 1$, are presented in Fig. 5 and listed in Table III as functions of the momentum transfer $-t$, for both the helicity and the Gottfried-Jackson frames.

To investigate the possible effect on these values of A_1 contamination we define the helicity angle θ_Δ as that angle between the Δ^{++} direction in the overall center of mass and the decay proton in the Δ^{++} rest frame. Events with $\cos\theta_\Delta < 0.0$ are inhibited kinematically from forming a $(\rho^0\pi^+)$ mass in the A_1 region, while events with $\cos\theta_\Delta > 0.0$ may correspond to A_1 reflection. A recalculation of the ρ^0 density matrix elements for both samples yields similar results, and we conclude that the A_1 background has no significant effect on the quoted values.

The single spin-density matrix elements of the $\Delta^{++}(1236)$, ρ_{33}, Re ρ_{31}, and Re ρ_{3-1} were also determined by the method of moments with no background subtraction. The observation that there is no change in these values when they are recalculated for events which cover a larger $(\pi^+\pi^-)$ mass interval leads us to conclude that our quoted values (see Fig. 5 and Table III) are unaffected by the $\pi^+\pi^-$ S-wave background.

As a check on the validity of our data we have verified that the conditions imposed on the density matrix elements by the positivity requirement were satisfied within statistical errors in each $-t$ interval.[9]

B. $\pi^+ p \to \omega \Delta^{++}(1236)$

For the determination of the spin-density matrix elements for reaction (2) the events in the overlap region of the ω and $\Delta^{++}(1236)$ (region γ) have been used.

The spin-density matrix elements of the ω meson (ρ^{00}, ρ^{1-1}, and Re ρ^{10}) and those of the $\Delta^{++}(1236)$ (ρ_{33}, Re ρ_{31}, and Re ρ_{3-1}) determined in the Gottfried-Jackson and helicity frames by the method of moments, are presented in Fig. 6 and listed in Table IV as functions of the momentum transfer $-t$.

Using events from the inner part of the ω Dalitz plot yields, within error, similar results; we conclude that the background under the ω meson does not influence our values. In a similar manner to that discussed earlier, we confirm that the B parity reflection has no significant influence on the ω density matrix elements, and we verify the positivity requirements within statistical errors.

Agreement between experiments at various energies[1,2] is generally close, with some differences in details, implying that the main production characteristics of both reactions (1) and (2) are stable over the range of beam momentum from 3 to 18 GeV/c.

We reserve a quantitative discussion of the natural- and unnatural-spin-parity contributions for Sec. VII.

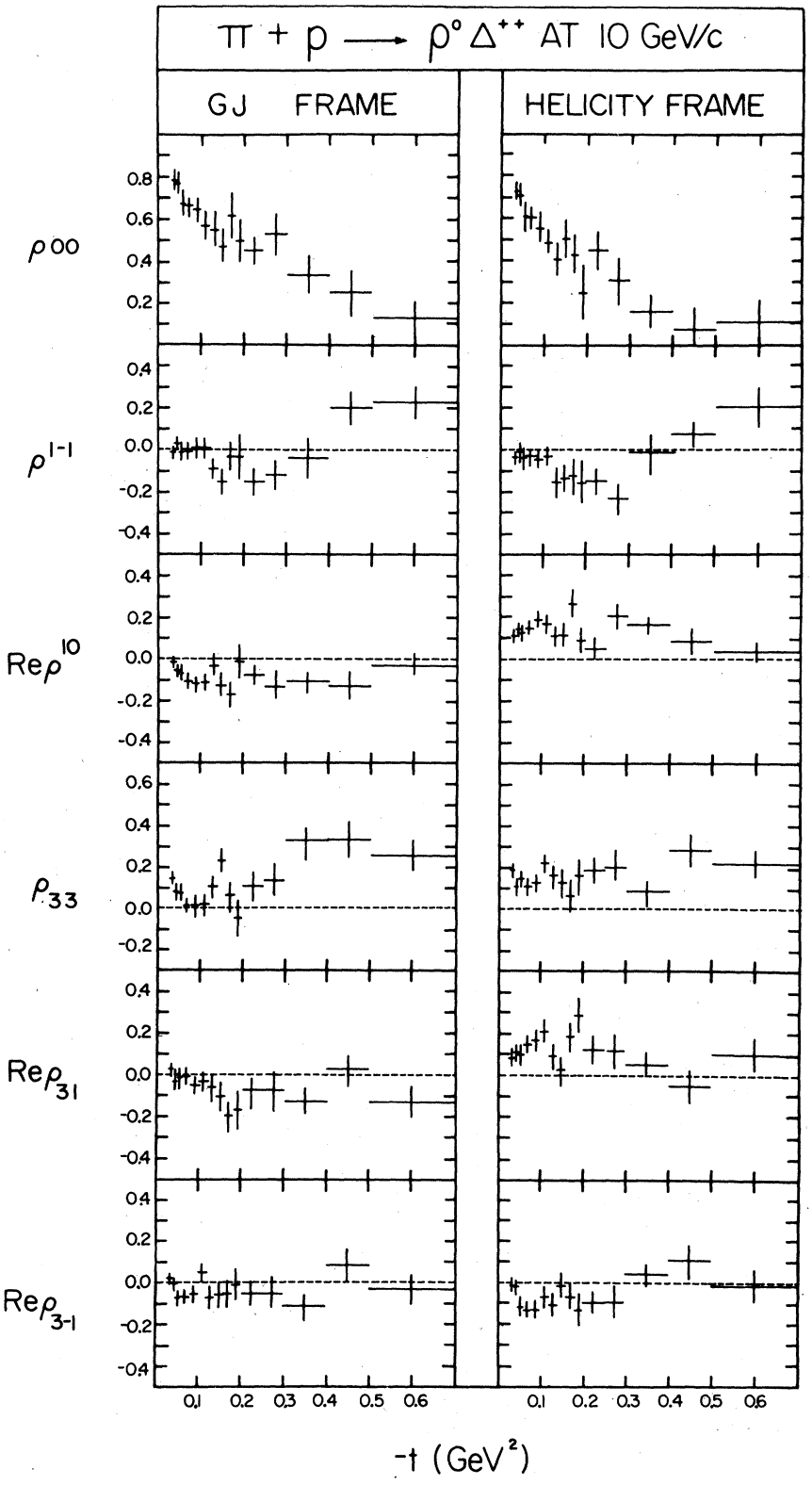

FIG. 5. Spin-density matrix elements of the ρ^0 and of the $\Delta^{++}(1236)$ as functions of $-t$ in the Gottfried-Jackson and helicity frames.

VI. JOINT SPIN-DENSITY MATRIX ELEMENTS AND JOINT DECAY CORRELATIONS

Besides the six single spin-density matrix elements discussed in Sec. V, joint spin-density matrix elements can be determined from the double resonance processes $\pi^+ p \to (\rho^0, \omega)\,\Delta^{++}(1236)$, as suggested by Pilkuhn and Svensson.[10] Parity conservation and Hermiticity of the spin-density matrix reduce the number of independent joint decay elements

$$\rho^{\lambda_V \lambda'_V}_{2\lambda_\Delta 2\lambda'_\Delta}$$

to 13. Table V summarizes the 13 independent combinations of

$$\rho^{\lambda_V \lambda'_V}_{2\lambda_\Delta 2\lambda_\Delta}$$

as well as their moments, renormalized so that the trace condition

$$\sum_{\lambda_\rho \lambda_\Delta} \rho^{\lambda_V \lambda_V}_{2\lambda_\Delta 2\lambda_\Delta} = 1$$

is fulfilled.

The 13 experimental moments for reaction (1) are presented as functions of $-t$ in the Gottfried-Jackson and helicity frames in Table VI. For reaction (2), the results presented in Table VII represent averages over the region $0.02 \leq -t \leq 0.6$ GeV^2.

As pointed out by Donohue,[11] the expression of Pilkuhn and Svensson for the joint decay distribution may be reexpressed as the product of the single-vertex distribution for $J^P = 1^-$ $[W_V(\theta_V, \phi_V)]$, $J^P = \frac{3}{2}^+$ $[W_\Delta(\theta_\Delta, \phi_\Delta)]$, and an additional ex-

TABLE III. Single spin-density matrix elements of (a) the ρ, and (b) the $\Delta^{++}(1236)$, as a function of $-t$ in the Gottfried-Jackson and helicity frames.

(a) ρ meson

	Gottfried-Jackson frame			Helicity frame		
$-t$ (GeV^2)	ρ^{00}	ρ^{1-1}	Re ρ^{10}	ρ^{00}	ρ^{1-1}	Re ρ^{10}
0.03–0.04	0.781 ± 0.046	−0.016 ± 0.029	−0.015 ± 0.030	0.735 ± 0.046	−0.039 ± 0.030	0.119 ± 0.029
0.04–0.05	0.772 ± 0.053	0.031 ± 0.036	−0.058 ± 0.035	0.713 ± 0.053	0.001 ± 0.038	0.143 ± 0.034
0.05–0.06	0.676 ± 0.062	−0.012 ± 0.044	−0.064 ± 0.041	0.619 ± 0.062	−0.040 ± 0.047	0.127 ± 0.039
0.06–0.08	0.665 ± 0.052	−0.005 ± 0.034	−0.104 ± 0.032	0.609 ± 0.055	−0.033 ± 0.034	0.155 ± 0.031
0.08–0.10	0.641 ± 0.059	0.006 ± 0.045	−0.118 ± 0.041	0.559 ± 0.069	−0.036 ± 0.044	0.198 ± 0.036
0.10–0.12	0.569 ± 0.070	0.011 ± 0.045	−0.114 ± 0.039	0.490 ± 0.065	−0.029 ± 0.046	0.172 ± 0.042
0.12–0.14	0.548 ± 0.081	−0.090 ± 0.055	−0.027 ± 0.053	0.413 ± 0.082	−0.157 ± 0.064	0.115 ± 0.048
0.14–0.16	0.472 ± 0.088	−0.151 ± 0.061	−0.122 ± 0.057	0.507 ± 0.091	−0.133 ± 0.064	0.118 ± 0.053
0.16–0.18	0.676 ± 0.109	−0.027 ± 0.072	−0.176 ± 0.064	0.488 ± 0.105	−0.121 ± 0.081	0.268 ± 0.062
0.18–0.20	0.499 ± 0.113	−0.028 ± 0.098	−0.011 ± 0.081	0.243 ± 0.130	−0.156 ± 0.105	0.094 ± 0.066
0.20–0.25	0.447 ± 0.077	−0.147 ± 0.064	−0.079 ± 0.057	0.451 ± 0.088	−0.145 ± 0.061	0.059 ± 0.054
0.25–0.30	0.559 ± 0.102	−0.121 ± 0.067	−0.129 ± 0.070	0.340 ± 0.114	−0.230 ± 0.078	0.212 ± 0.056
0.30–0.40	0.338 ± 0.090	−0.029 ± 0.068	−0.103 ± 0.045	0.158 ± 0.079	−0.008 ± 0.080	0.170 ± 0.043
0.40–0.50	0.317 ± 0.108	0.226 ± 0.099	−0.124 ± 0.065	0.041 ± 0.120	0.078 ± 0.088	0.093 ± 0.066
0.50–0.70	0.134 ± 0.097	0.223 ± 0.087	−0.023 ± 0.054	0.107 ± 0.094	0.209 ± 0.091	0.041 ± 0.053

(b) $\Delta^{++}(1236)$

	Gottfried-Jackson frame			Helicity frame		
$-t$ (GeV^2)	ρ_{33}	Re ρ_{31}	Re ρ_{3-1}	ρ_{33}	Re ρ_{31}	Re ρ_{3-1}
0.03–0.04	0.144 ± 0.035	0.029 ± 0.034	0.023 ± 0.031	0.186 ± 0.033	0.087 ± 0.036	−0.001 ± 0.032
0.04–0.05	0.082 ± 0.039	−0.026 ± 0.043	−0.005 ± 0.035	0.104 ± 0.040	0.107 ± 0.041	−0.018 ± 0.036
0.05–0.06	0.079 ± 0.042	−0.017 ± 0.051	−0.071 ± 0.042	0.144 ± 0.047	0.100 ± 0.046	−0.108 ± 0.043
0.06–0.08	0.014 ± 0.039	−0.013 ± 0.042	−0.066 ± 0.032	0.116 ± 0.042	0.153 ± 0.039	−0.125 ± 0.034
0.08–0.10	0.017 ± 0.049	−0.050 ± 0.049	−0.057 ± 0.040	0.132 ± 0.049	0.174 ± 0.049	−0.124 ± 0.041
0.10–0.12	0.019 ± 0.051	−0.031 ± 0.049	0.056 ± 0.043	0.225 ± 0.047	0.213 ± 0.049	−0.063 ± 0.047
0.12–0.14	0.106 ± 0.059	−0.060 ± 0.062	−0.069 ± 0.052	0.162 ± 0.061	0.092 ± 0.061	−0.101 ± 0.051
0.14–0.16	0.225 ± 0.063	−0.101 ± 0.068	−0.059 ± 0.063	0.130 ± 0.069	0.031 ± 0.064	−0.004 ± 0.060
0.16–0.18	0.061 ± 0.079	−0.200 ± 0.077	−0.056 ± 0.063	0.072 ± 0.082	0.186 ± 0.074	−0.063 ± 0.063
0.18–0.20	−0.045 ± 0.083	−0.168 ± 0.092	−0.003 ± 0.074	0.162 ± 0.090	0.295 ± 0.084	−0.123 ± 0.076
0.20–0.25	0.114 ± 0.064	−0.069 ± 0.061	−0.049 ± 0.056	0.192 ± 0.064	0.131 ± 0.062	−0.094 ± 0.057
0.25–0.30	0.138 ± 0.082	−0.071 ± 0.079	−0.048 ± 0.076	0.211 ± 0.077	0.123 ± 0.083	−0.090 ± 0.077
0.30–0.40	0.333 ± 0.059	−0.128 ± 0.065	−0.101 ± 0.056	0.081 ± 0.060	0.056 ± 0.065	0.044 ± 0.054
0.40–0.50	0.334 ± 0.080	0.033 ± 0.074	0.085 ± 0.085	0.292 ± 0.082	−0.041 ± 0.073	0.109 ± 0.084
0.50–0.70	0.259 ± 0.070	−0.125 ± 0.079	−0.025 ± 0.067	0.224 ± 0.067	0.116 ± 0.079	−0.005 ± 0.071

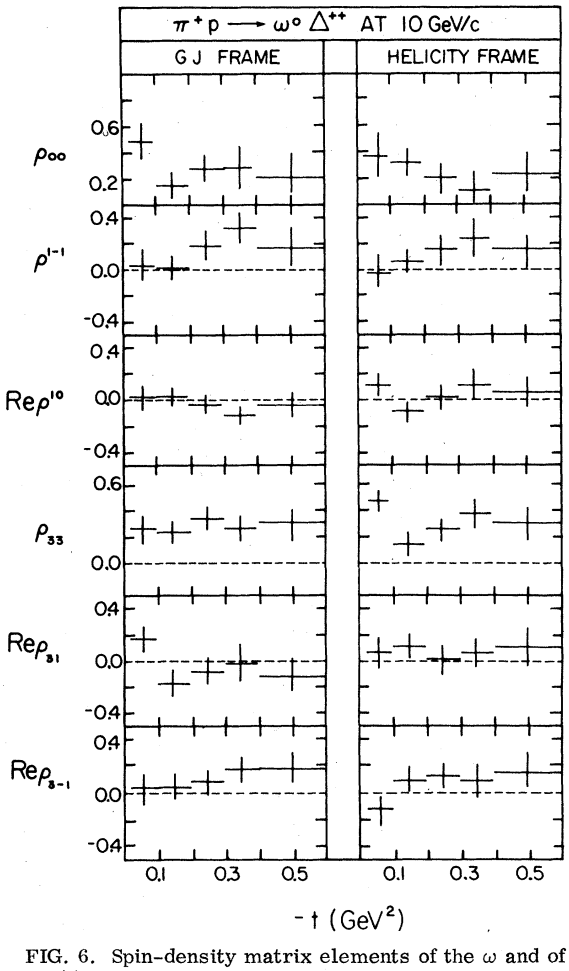

FIG. 6. Spin-density matrix elements of the ω and of the $\Delta^{++}(1236)$ as functions of $-t$ in the Gottfried-Jackson and helicity frames.

pression, I, that measures the correlation between the vector-meson and the Δ^{++} decays:

$$W(\theta_V, \phi_V, \theta_\Delta, \phi_\Delta) = W_V(\theta_V, \phi_V) W_\Delta(\theta_\Delta, \phi_\Delta) + I(\theta_V, \phi_V, \theta_\Delta, \phi_\Delta) \quad (20)$$

with

$$I(\theta_V, \phi_V, \theta_\Delta, \phi_\Delta) = \sum_{\substack{\lambda_\rho \lambda'_\rho \\ \lambda_\Delta \lambda'_\Delta}} (\rho^{\lambda_\rho \lambda'_\rho}_{2\lambda_\Delta 2\lambda'_\Delta} - \rho^{\lambda_\rho \lambda'_\rho}\rho_{2\lambda_\Delta 2\lambda'_\Delta}) \times U^{\lambda_\rho \lambda'_\rho}(\theta_V, \phi_V) \times V_{2\lambda_\Delta 2\lambda'_\Delta}(\theta_\Delta, \phi_\Delta),$$

where $U^{\lambda_\rho \lambda'_\rho}(\theta_V, \phi_V)$ and $V_{2\lambda_\Delta 2\lambda'_\Delta}(\theta_\Delta, \phi_\Delta)$ represent bilinear forms of the corresponding resonance decay amplitudes. The expression for the 13 independent correlation coefficients is given in Table VIII and their values for reaction (1) are shown in Fig. 7 as functions of $-t$.

It may be seen that most of the correlation terms do not differ significantly from zero in either frame. The coefficient, $D_1 \sim (1 - 3\cos^2\theta_V) \times (1 - 3\cos^2\theta_\Delta)$, shows significant departure from zero in the Gottfried-Jackson frame, indicating a strong correlation between the polar angles of the π^+ from the ρ^0 decay and the proton from $\Delta^{++}(1236)$ decay. Direct evidence for this correlation is shown in Fig. 8, where the ρ and Δ decay angles in the Gottfried-Jackson frame are plotted separately for the equatorial and polar regions of the other angle, for $-t < 0.1$ GeV^2. The most striking difference occurs in the shape of the $\cos\theta_\Delta$ distribution for ρ^0 decays in the

TABLE IV. Single spin-density matrix elements of (a) the ω and, (b) the $\Delta^{++}(1236)$, as a function of $-t$ in the Gottfried-Jackson and helicity frames.

(a) ω meson

	Gottfried-Jackson frame			Helicity frame		
$-t$ (GeV^2)	ρ^{00}	ρ^{1-1}	$\mathrm{Re}\rho^{10}$	ρ^{00}	ρ^{1-1}	$\mathrm{Re}\rho^{10}$
0.02–0.10	0.493 ± 0.154	0.042 ± 0.125	0.011 ± 0.104	0.387 ± 0.175	−0.011 ± 0.127	0.127 ± 0.088
0.10–0.20	0.158 ± 0.100	0.010 ± 0.099	0.015 ± 0.065	0.284 ± 0.109	0.073 ± 0.083	−0.098 ± 0.070
0.20–0.30	0.274 ± 0.102	0.192 ± 0.106	−0.013 ± 0.090	0.204 ± 0.126	0.156 ± 0.117	0.035 ± 0.069
0.30–0.40	0.277 ± 0.187	0.325 ± 0.128	−0.109 ± 0.082	0.123 ± 0.135	0.248 ± 0.160	0.126 ± 0.092
0.40–0.60	0.214 ± 0.171	0.171 ± 0.157	−0.045 ± 0.109	0.247 ± 0.160	0.188 ± 0.162	0.068 ± 0.111

(b) $\Delta^{++}(1236)$

	Gottfried-Jackson frame			Helicity frame		
$-t$ (GeV^2)	ρ_{33}	$\mathrm{Re}\,\rho_{31}$	$\mathrm{Re}\,\rho_{31}$	ρ_{33}	$\mathrm{Re}\,\rho_{31}$	$\mathrm{Re}\,\rho_{3-}$
0.02–0.10	0.256 ± 104	0.176 ± 0.112	0.012 ± 0.130	0.458 ± 0.086	0.077 ± 0.106	−0.104 ± 0.146
0.10–0.20	0.248 ± 0.088	−0.181 ± 0.091	0.037 ± 0.068	0.149 ± 0.085	0.126 ± 0.079	0.094 ± 0.085
0.20–0.30	0.345 ± 0.090	−0.078 ± 0.093	0.084 ± 0.101	0.259 ± 0.095	0.018 ± 0.096	0.133 ± 0.094
0.30–0.40	0.260 ± 0.113	−0.017 ± 0.140	0.169 ± 0.117	0.392 ± 0.112	0.057 ± 0.126	0.093 ± 0.131
0.40–0.60	0.310 ± 0.125	−0.119 ± 0.125	0.177 ± 0.141	0.358 ± 0.118	0.122 ± 0.134	0.150 ± 0.139

TABLE V. The 13 independent measurable combinations of joint spin-density matrix elements and their moments.

$$R_1 = \rho^-_{33} - \rho^-_{11} = \tfrac{25}{8}\langle(1-3\cos^2\theta_V)(1-3\cos^2\theta_\Delta)\rangle$$
$$R_2 = \rho^{1-1} = -\tfrac{25}{8}\langle\sin^2\theta_V\cos2\phi_V(1-3\cos^2\theta_\Delta)\rangle$$
$$R_3 = \mathrm{Re}\rho^{10} = \left(\frac{25}{8\sqrt{2}}\right)\langle\sin2\theta_V\cos\phi_V(1-3\cos^2\theta_\Delta)\rangle$$
$$R_4 = \mathrm{Re}\rho^-_{3-1} = -\tfrac{25}{16}\sqrt{3}\,\langle(1-3\cos^2\theta_V)\sin^2\theta_\Delta\cos2\phi_\Delta\rangle$$
$$R_5 = \mathrm{Re}\rho^-_{31} = -\tfrac{25}{16}\sqrt{3}\,\langle(1-3\cos^2\theta_V)\sin2\theta_\Delta\cos^2\phi_\Delta\rangle$$
$$R_6 = \mathrm{Re}\rho^{1-1}_{3-1} = \tfrac{25}{32}\sqrt{3}\,\langle\sin^2\theta_V\sin^2\theta_\Delta\cos2(\phi_V+\phi_\Delta)\rangle$$
$$R_7 = \mathrm{Re}\rho^{-11}_{3-1} = \tfrac{25}{32}\sqrt{3}\,\langle\sin^2\theta_V\sin^2\theta_\Delta\cos(2\phi_V-\phi_\Delta)\rangle$$
$$R_8 = \mathrm{Re}\rho^{1-1}_{31} = \tfrac{25}{32}\sqrt{3}\,\langle\sin^2\theta_V\sin2\theta_\Delta\cos(2\phi_V+\phi_\Delta)\rangle$$
$$R_9 = \mathrm{Re}\rho^{-11}_{31} = \tfrac{25}{32}\sqrt{3}\,\langle\sin^2\theta_V\sin2\theta_\Delta\cos(2\phi_V-\phi_\Delta)\rangle$$
$$R_{10} = \mathrm{Re}(\rho^{10}_{3-1} - \rho^{0-1}_{3-1}) = \tfrac{25}{32}\sqrt{6}\,\langle\sin2\theta_V\sin^2\theta_\Delta\cos(\phi_V+2\phi_\Delta)\rangle$$
$$R_{11} = \mathrm{Re}(\rho^{01}_{3-1} - \rho^{-10}_{3-1}) = \tfrac{25}{32}\sqrt{6}\,\langle\sin2\theta_V\sin^2\theta_\Delta\cos(\phi_V-2\phi_\Delta)\rangle$$
$$R_{12} = \mathrm{Re}(\rho^{10}_{31} - \rho^{0-1}_{31}) = \tfrac{25}{32}\sqrt{6}\,\langle\sin2\theta_V\sin2\theta_\Delta\cos(\phi_V+\phi_\Delta)\rangle$$
$$R_{13} = \mathrm{Re}(\rho^{01}_{31} - \rho^{-10}_{31}) = \tfrac{25}{32}\sqrt{6}\,\langle\sin2\theta_V\sin2\theta_\Delta\cos(\phi_V-\phi_\Delta)\rangle$$

where $\rho^-_{nn'} = \rho^{11}_{nn'} + \rho^{-1-1}_{nn'} - 2\rho^{00}_{nn'}$,

$$\rho^{m\,m'}_{---} = \rho^{m\,m'}_{33} + \rho^{m\,m'}_{-3-3} - \rho^{m\,m'}_{11} - \rho^{m\,m'}_{-1-1}$$

equatorial region, where the data deviate strongly from the simple form $(1+3\cos^2\theta_\Delta)$.

The correlation coefficients of reaction (2) are presented in Table VII. Although the statistical significance of any correlations between the ω and $\Delta^{++}(1236)$ decays is poor, some coefficients are approximately two standard deviations away from zero. As for reaction (1), D_1 is different from zero in the Gottfried-Jackson frame which indicates a correlation between the polar angles of the ω^0 and $\Delta^{++}(1236)$ decays.

Analogous results have been obtained at 3.7 (Refs. 1i and 2h), 5.0 (Refs. 1m and 2k), 13.0 (Refs. 1v and 2s), and 16.0 (Refs. 1w and 2t) GeV/c.

To check the validity of our data we have compared our results with the positivity requirement for the joint spin-density matrix elements proposed by Donohue *et al.*[12] In our data small violations of the positivity condition are observed, although they lie within our estimates of error. The observation that our experimental points lie just "outside" the boundary of the positivity domain is discussed in Sec. IX.

TABLE VI. Combinations of the joint density matrix elements of the ρ^0 and of the $\Delta^{++}(1236)$ as a function of $-t$ in (a) the Gottfried-Jackson, and (b) the helicity frames. For clarity the values which differ from zero by more than one standard deviation have been underlined.

$-t$ (GeV^2)	0.03–0.04	0.04–0.06	0.06–0.10	0.10–0.15	0.15–0.30	0.30–0.60
			(a) Gottfried-Jackson frame			
R_1	0.496 ± 0.105	0.271 ± 0.088	0.592 ± 0.086	0.245 ± 0.094	0.543 ± 0.081	−0.236 ± 0.107
R_2	−0.032 ± 0.064	0.137 ± 0.061	−0.022 ± 0.069	0.048 ± 0.078	0.066 ± 0.081	0.174 ± 0.111
R_3	−0.035 ± 0.069	0.014 ± 0.061	−0.123 ± 0.069	−0.014 ± 0.076	0.165 ± 0.075	0.152 ± 0.073
R_4	−0.174 ± 0.083	0.082 ± 0.069	0.024 ± 0.066	−0.041 ± 0.088	0.153 ± 0.071	0.088 ± 0.105
R_5	0.005 ± 0.093	0.060 ± 0.084	0.123 ± 0.085	0.149 ± 0.089	0.198 ± 0.088	0.321 ± 0.100
R_6	0.034 ± 0.023	0.022 ± 0.018	0.005 ± 0.017	0.048 ± 0.022	0.013 ± 0.025	0.016 ± 0.040
R_7	−0.003 ± 0.023	−0.022 ± 0.018	0.006 ± 0.019	−0.019 ± 0.025	0.024 ± 0.024	0.038 ± 0.039
R_8	−0.003 ± 0.024	0.034 ± 0.023	0.005 ± 0.021	−0.027 ± 0.028	−0.014 ± 0.027	−0.070 ± 0.038
R_9	−0.048 ± 0.025	−0.034 ± 0.023	−0.041 ± 0.022	0.006 ± 0.029	0.021 ± 0.027	−0.056 ± 0.039
R_{10}	−0.001 ± 0.043	−0.023 ± 0.039	0.025 ± 0.033	0.037 ± 0.042	0.002 ± 0.043	0.046 ± 0.061
R_{11}	−0.049 ± 0.044	0.003 ± 0.037	0.009 ± 0.036	0.035 ± 0.042	0.074 ± 0.044	−0.026 ± 0.061
R_{12}	−0.083 ± 0.049	−0.094 ± 0.049	−0.164 ± 0.042	−0.042 ± 0.051	−0.101 ± 0.049	0.063 ± 0.058
R_{13}	−0.024 ± 0.051	−0.017 ± 0.046	0.111 ± 0.044	0.054 ± 0.047	0.003 ± 0.046	−0.132 ± 0.061
			(b) Helicity frame			
R_1	0.181 ± 0.095	0.111 ± 0.075	0.254 ± 0.087	0.175 ± 0.088	0.175 ± 0.087	−0.284 ± 0.096
R_2	−0.026 ± 0.063	0.162 ± 0.071	0.011 ± 0.067	0.020 ± 0.078	0.131 ± 0.089	0.181 ± 0.122
R_3	0.126 ± 0.066	0.132 ± 0.064	0.174 ± 0.064	0.038 ± 0.071	0.161 ± 0.072	0.121 ± 0.084
R_4	−0.106 ± 0.089	0.096 ± 0.073	0.116 ± 0.075	0.072 ± 0.076	−0.001 ± 0.079	0.241 ± 0.101
R_5	−0.232 ± 0.089	−0.102 ± 0.080	−0.212 ± 0.085	−0.014 ± 0.095	0.166 ± 0.088	0.316 ± 0.098
R_6	0.024 ± 0.024	0.002 ± 0.021	−0.049 ± 0.021	0.012 ± 0.027	0.039 ± 0.028	0.070 ± 0.040
R_7	0.013 ± 0.024	0.002 ± 0.021	0.052 ± 0.021	0.005 ± 0.025	0.065 ± 0.025	−0.064 ± 0.041
R_8	0.017 ± 0.027	0.035 ± 0.024	0.061 ± 0.022	0.005 ± 0.028	−0.037 ± 0.028	−0.068 ± 0.046
R_9	−0.034 ± 0.026	−0.067 ± 0.022	−0.049 ± 0.022	−0.044 ± 0.029	−0.093 ± 0.030	0.007 ± 0.046
R_{10}	0.044 ± 0.042	0.002 ± 0.038	0.077 ± 0.036	−0.087 ± 0.047	−0.004 ± 0.039	0.088 ± 0.052
R_{11}	−0.010 ± 0.043	−0.009 ± 0.038	−0.068 ± 0.035	−0.035 ± 0.048	−0.065 ± 0.041	0.093 ± 0.051
R_{12}	−0.016 ± 0.049	−0.042 ± 0.045	−0.031 ± 0.036	0.013 ± 0.047	−0.029 ± 0.043	−0.026 ± 0.059
R_{13}	0.006 ± 0.053	−0.022 ± 0.044	0.105 ± 0.039	0.016 ± 0.047	0.056 ± 0.041	0.019 ± 0.049

TABLE VII. Combinations of the joint density matrix elements of the ω and of the $\Delta^{++}(1236)$ in (a) the Gottfried-Jackson, and (b) the helicity frames for the $-t$ range 0.02–0.60 GeV^2. The correlation coefficients are also presented. For clarity the values which differ from zero by more than one standard deviation have been underlined.

(a) Gottfried-Jackson frame

R_1	$\underline{0.208 \pm 0.101}$	D_1	$\underline{0.195 \pm 0.101}$
R_2	$\underline{0.167 \pm 0.099}$	D_2	$\underline{0.151 \pm 0.114}$
R_3	-0.025 ± 0.085	D_3	-0.023 ± 0.097
R_4	$\underline{-0.114 \pm 0.106}$	D_4	$\underline{0.130 \pm 0.118}$
R_5	0.083 ± 0.093	D_5	0.096 ± 0.111
R_6	$\underline{0.136 \pm 0.046}$	D_6	$\underline{0.126 \pm 0.071}$
R_7	-0.031 ± 0.045	D_7	-0.041 ± 0.071
R_8	0.038 ± 0.048	D_8	0.046 ± 0.072
R_9	0.006 ± 0.046	D_9	0.014 ± 0.071
R_{10}	-0.017 ± 0.066	D_{10}	-0.014 ± 0.081
R_{11}	0.022 ± 0.067	D_{11}	0.025 ± 0.082
R_{12}	-0.011 ± 0.069	D_{12}	-0.013 ± 0.086
R_{13}	0.027 ± 0.072	D_{13}	0.025 ± 0.087

(b) Helicity frame

R_1	$\underline{0.122 \pm 0.102}$	D_1	$\underline{0.103 \pm 0.102}$
R_2	0.048 ± 0.076	D_2	0.029 ± 0.088
R_3	-0.048 ± 0.076	D_3	-0.053 ± 0.089
R_4	$\underline{0.254 \pm 0.106}$	D_4	$\underline{0.236 \pm 0.123}$
R_5	-0.034 ± 0.103	D_5	-0.053 ± 0.121
R_6	0.023 ± 0.046	D_6	0.014 ± 0.071
R_7	0.002 ± 0.048	D_7	-0.007 ± 0.073
R_8	$\underline{0.064 \pm 0.048}$	D_8	0.054 ± 0.073
R_9	$\underline{-0.102 \pm 0.046}$	D_9	$\underline{-0.112 \pm 0.072}$
R_{10}	$\underline{0.101 \pm 0.066}$	D_{10}	$\underline{0.097 \pm 0.083}$
R_{11}	-0.031 ± 0.058	D_{11}	-0.035 ± 0.077
R_{12}	$\underline{0.166 \pm 0.067}$	D_{12}	$\underline{0.162 \pm 0.082}$
R_{13}	0.004 ± 0.066	D_{13}	-0.001 ± 0.080

TABLE VIII. The 13 independent correlation coefficients expressed by the single and joint spin-density matrix elements.

$$D_1 = (\rho^-_{33} - \rho^-_{11}) - \tfrac{1}{2}(3\rho^{00} - 1)(1 - 4\rho_{33})$$
$$D_2 = \rho^{1-1}_{-} - (4\rho_{33} - 1)\rho^{1-1}$$
$$D_3 = \mathrm{Re}\,\rho^{10}_{-} - (4\rho_{33} - 1)\,\mathrm{Re}\,\rho^{10}$$
$$D_4 = \mathrm{Re}\,\rho^-_{3-1} - (1 - 3\rho^{00})\,\mathrm{Re}\,\rho_{3-1}$$
$$D_5 = \mathrm{Re}\,\rho^-_{31} - (1 - 3\rho^{00})\,\mathrm{Re}\,\rho_{31}$$
$$D_6 = \mathrm{Re}\,\rho^{1-1}_{3-1} - \rho^{1-1}\,\mathrm{Re}\,\rho_{3-1}$$
$$D_7 = \mathrm{Re}\,\rho^{-11}_{3-1} - \rho^{1-1}\,\mathrm{Re}\,\rho_{3-1}$$
$$D_8 = \mathrm{Re}\,\rho^{1-1}_{31} - \rho^{1-1}\,\mathrm{Re}\,\rho_{31}$$
$$D_9 = \mathrm{Re}\,\rho^{-11}_{31} - \rho^{1-1}\,\mathrm{Re}\,\rho_{31}$$
$$D_{10} = \mathrm{Re}(\rho^{10}_{3-1} - \rho^{0-1}_{3-1}) - 2\,\mathrm{Re}\,\rho^{10}\,\mathrm{Re}\,\rho_{3-1}$$
$$D_{11} = \mathrm{Re}(\rho^{01}_{3-1} - \rho^{-10}_{3-1}) - 2\,\mathrm{Re}\,\rho^{10}\,\mathrm{Re}\,\rho_{3-1}$$
$$D_{12} = \mathrm{Re}(\rho^{10}_{31} - \rho^{0-1}_{31}) - 2\,\mathrm{Re}\,\rho^{10}\,\mathrm{Re}\,\rho_{31}$$
$$D_{13} = \mathrm{Re}(\rho^{01}_{31} - \rho^{-10}_{31}) - 2\,\mathrm{Re}\,\rho^{10}\,\mathrm{Re}\,\rho_{31}$$

VII. NATURAL- AND UNNATURAL-SPIN-PARITY EXCHANGE

As shown in Ref. 13, the quantities $\sigma^{1\pm} = \rho^{11} \pm \rho^{1-1}$ and $\sigma^{0-} = \rho^{00}$ give asymptotically the relative contributions of natural (+) and unnatural (-) spin-parity exchange, respectively, to vector-meson helicity-one and helicity-zero states, while $\sigma^- = \sigma^{0-} + \sigma^{1-}$ gives the total amount of unnatural-spin-parity exchange.

The quantities $\sigma^{m\pm}$ do not contain information about the $\Delta^{++}(1236)$ helicity states. By means of the joint spin-density matrix elements, it is possible to extract the relative amount of spin-parity exchanges leading to definite helicity states of the vector meson, as well as of the $\Delta^{++}(1236)$. These quantities are defined by[14]

$$\sigma^{m\pm}_{2n} = \tfrac{1}{4} \sum_{\substack{\lambda_\rho = \pm m \\ \lambda_\Delta = \pm n}} [\rho^{\lambda_\rho \lambda_\rho}_{2\lambda_\Delta 2\lambda_\Delta} + \rho^{-\lambda_\rho - \lambda_\rho}_{2\lambda_\Delta 2\lambda_\Delta} \pm (-1)^{\lambda_\rho + 1}\, 2\,\mathrm{Re}\,\rho^{\lambda_\rho - \lambda_\rho}_{2\lambda_\Delta 2\lambda_\Delta}]. \qquad (21)$$

In order to minimize the errors on the $\sigma^{m\pm}$ and $\sigma^{m\pm}_{2n}$, the method of moments was used. σ^{1-} and the $\sigma^{m\pm}_{2n}$ were evaluated in the Gottfried-Jackson (GJ) and helicity (H) frames; σ^{1+} and σ^- are invariant under transformations between these frames.

A. $\pi^+ p \to \rho^0 \Delta^{++}(1236)$

The different contributions of the natural-spin-parity (NP) exchange and unnatural-spin-parity (UNP) exchange are presented in Fig. 9 as functions of the momentum transfer $-t$ for the reaction $\pi^+ p \to \rho^0 \Delta^{++}(1236)$.

From these distributions and the $\rho^{mm'}$ distributions presented previously in Fig. 5, the following observations can be made on their behavior as functions of $-t$:

(a) In both frames, ρ^{00} is large at small $-t$ and σ^{0-}_1 is approximately equal to ρ^{00} for $-t \leq 0.3$ GeV^2. Beyond this value of $-t$, σ^{0-}_3 becomes greater than σ^{0-}_1. We note also that ρ^{00}_H decreases more rapidly than does the corresponding ρ^{00}_{GJ} distribution.

(b) ρ^{1-1}_{GJ} and ρ^{1-1}_H are observed to be negative for $-t \leq 0.4$ GeV^2 and positive in the larger $-t$ region. Moreover, one sees that $|\rho^{1-1}_H| > |\rho^{1-1}_{GJ}|$ for almost the whole range of $-t$ considered.

(c) $\mathrm{Re}\,\rho^{10}_H$ increases more rapidly than $\mathrm{Re}\,\rho^{10}_{GJ}$ decreases in the small $-t$ region.

(d) σ^- is large at small $-t$ having an approximately constant value of 0.85 for $-t \leq 0.3$ GeV^2. σ^- is approximately equal to ρ^{00} in the forward direction ($-t \leq 0.1$ GeV^2).

(e) A small, but significant value of σ^{1+} is ob-

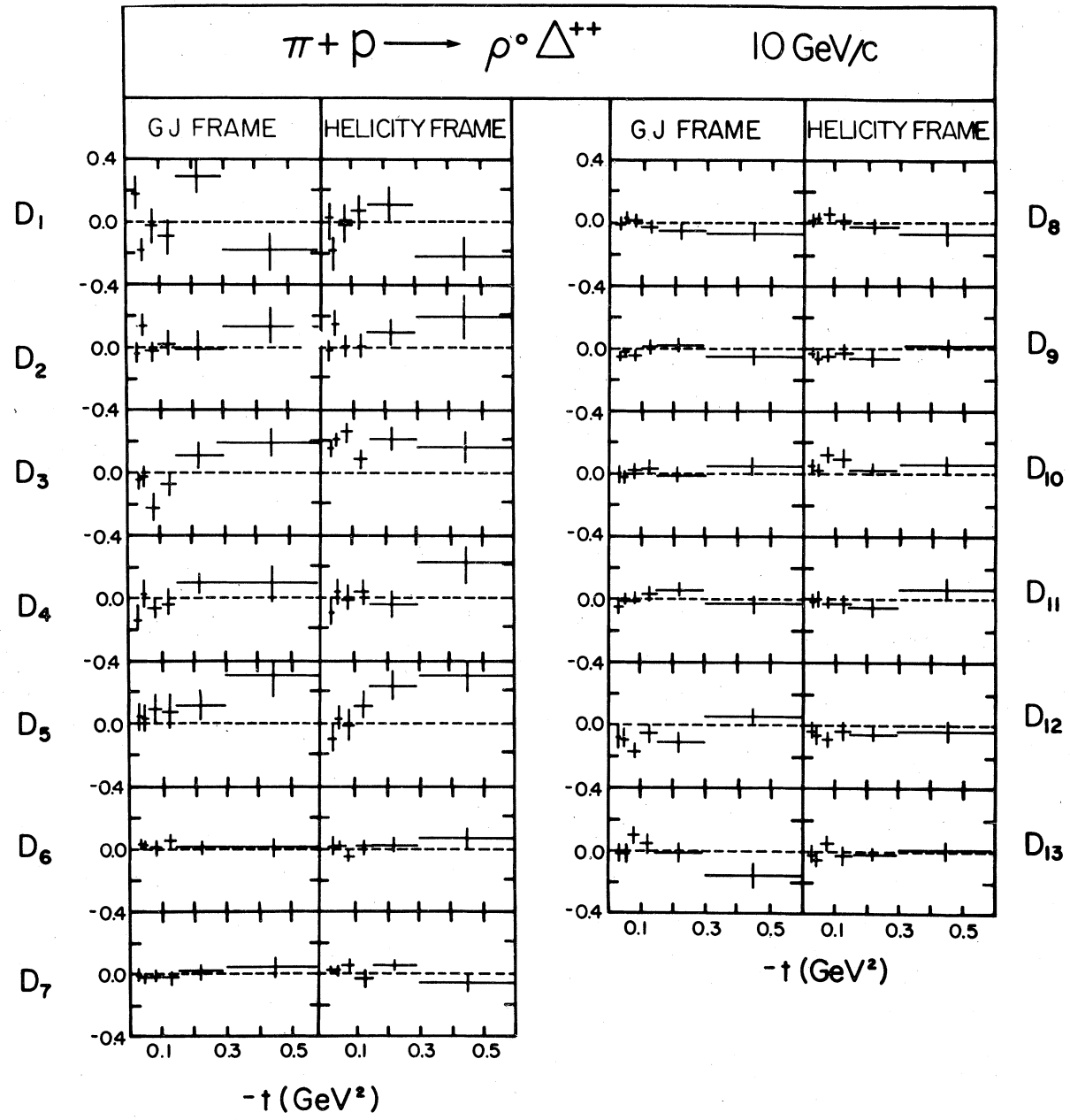

FIG. 7. Correlation coefficients of the ρ^0 and of the Δ^{++} (1236) decay angular distributions as functions of $-t$ in the Gottfried-Jackson and helicity frames.

served for $-t < 0.3$ GeV^2. Beyond this value of $-t$, σ^{1+} increases with $\sigma^{1+}_{3GJ} > \sigma^{1+}_{1GJ}$ and $\sigma^{1+}_{3H} \simeq \sigma^{1+}_{1H}$.

(f) σ^{1-} rises rapidly from a significantly nonzero value at low $-t$ to a maximum at $-t \simeq 0.3$ GeV^2 and decreases beyond this value. For almost all $-t$ values, σ^{1-}_{GJ} is smaller than σ^{1-}_{H}. In both frames, σ^{1-}_{1} is greater than σ^{1-}_{3} for $-t \geq 0.3$ GeV^2.

The behavior of ρ^{mm}, $\sigma^{m\pm}$, and $\sigma^{m\pm}_{2n}$ discussed above leads to the conclusion that the reaction $\pi^+ p \to \rho^0 \Delta^{++}(1236)$ is dominated by the UNP-exchange contribution for $-t$ less than 0.3 GeV^2. However, although σ^- and ρ^{00} are large at small momentum transfers and the other elements are small, neither actually reaches the one-particle-exchange predictions for 0^- exchange: $\rho^{00} = 1$, $\rho^{10} = \rho^{1-1} = \rho_{33} = \rho_{31} = \rho_{3-1} = 0$. Moreover, from the large value of σ^{0-}_{1} at small $-t$, one can conclude that the UNP exchange leading to $\lambda_\rho = 0$ and λ_Δ

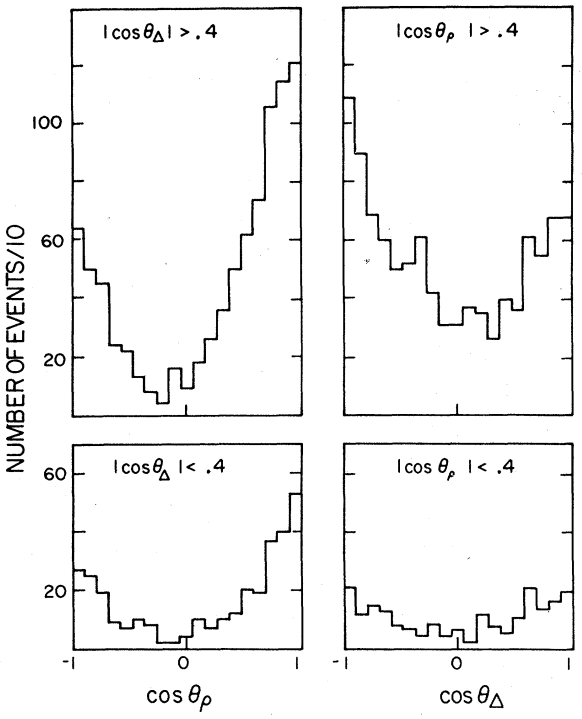

FIG. 8. Gottfried-Jackson angle distributions of θ_ρ and θ_Δ for polar and equatorial bands in θ_Δ and θ_ρ, respectively, for $-t < 0.1$ GeV^2.

$= \pm\frac{1}{2}$ helicity states is the dominant contribution in this momentum transfer region.

With increasing momentum transfer, the NP-exchange contribution increases, as shown by increasing values of σ^{1+} and positive values of ρ^{1-1} ($2\rho^{1-1} \simeq$ NP $-$ UNP). At $-t \simeq 0.45$ GeV^2, the NP-exchange contribution is approximately equal to that from the UNP exchange. However, this contribution never reaches the limit of elementary NP exchange ($\rho^{1\,-1} = \frac{1}{2}$, $\rho^{00} = \rho^{10} = 0$). In the helicity frame, NP exchange leads to, approximately, equal productions of $\lambda_\Delta = \pm\frac{3}{2}$ and $\lambda_\Delta = \pm\frac{1}{2}$ helicity states.

Finally, even at small $-t$, there is still a significant UNP contribution to helicity-one ρ^0 states, which reaches its maximum at $-t \simeq 0.3$ GeV^2. This contribution is mainly associated with the $\Delta^{++}(1236)$ $\pm\frac{1}{2}$ helicity states.

Table IX summarizes the cross section for measurable exchanges in reaction (1) integrated over momentum transfer up to $-t = 0.6$ GeV^2.

In this $-t$ region the NP-exchange contributions represent 13% of the $\rho^0\Delta^{++}(1236)$ cross section of Eq. (7). 57% of this cross section is due to UNP exchange leading to $\lambda_\rho = 0$ and $\lambda_\Delta = \pm\frac{1}{2}$ helicity states, while only 16% of the UNP-exchange contribution leads to $\lambda_\rho = \pm 1$ helicity states,

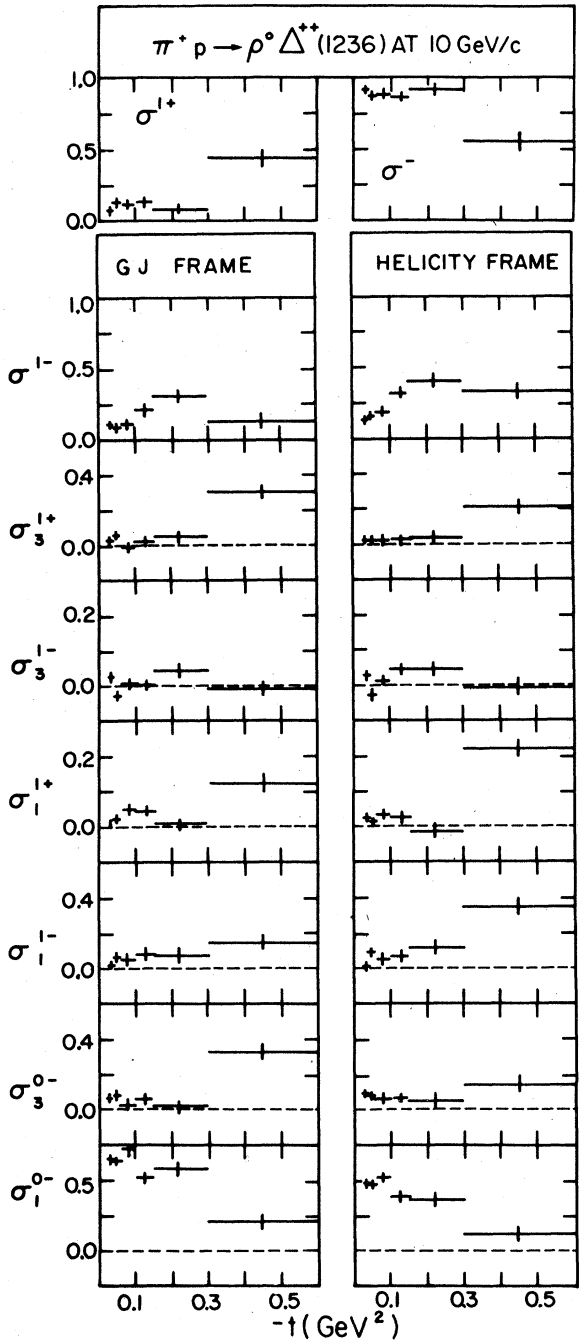

FIG. 9. Relative proportion of the natural-spin-parity exchange σ^{1+}; the unnatural-spin-parity exchange, σ^-; the unnatural-spin-parity exchange to ρ^0 helicity ± 1, σ^{1-}; the natural-spin-parity exchange to ρ^0 helicity ± 1 and Δ^{++} helicity $\pm\frac{3}{2}$, σ_3^{1+}; the unnatural-spin-parity exchange to ρ^0 helicity ± 1 and Δ^{++} helicity $\pm\frac{3}{2}$, σ_3^{1-}; the natural-spin-parity exchange to ρ^0 helicity ± 1 and Δ^{++} helicity $\pm\frac{1}{2}$, σ_1^{1+}; the unnatural-spin-parity exchange to ρ^0 helicity ± 1 and Δ^{++} helicity $\pm\frac{1}{2}$, σ_1^{1-}; the unnatural-spin-parity exchange to ρ^0 helicity 0 and Δ^{++} helicity $\pm\frac{3}{2}$, σ_3^{0-}; the unnatural-spin-parity exchange to ρ^0 helicity 0 and Δ^{++} helicity $\pm\frac{1}{2}$, σ_1^{0-}.

TABLE IX. Cross sections (in μb) of the measurable exchanges in the reactions $\pi^+p \to \rho^0\Delta^{++}(1236)$ and $\pi^+p \to \omega\Delta^{++}(1236)$ in the Gottfried-Jackson and helicity frames.

	$\pi^+p \to \rho^0\Delta^{++}(1236)$		$\pi^+p \to \omega^0\Delta^{++}(1236)$	
	GJ frame	Helicity frame	GJ frame	Helicity frame
$\int \sigma^{-} \frac{d\sigma}{dt} dt$	340 ± 16	340 ± 16	33 ± 4	33 ± 4
$\int \sigma^{1-} \frac{d\sigma}{dt} dt$	61 ± 6	62 ± 6	15 ± 4	16 ± 4
$\int \sigma^{1+} \frac{d\sigma}{dt} dt$	54 ± 6	54 ± 6	31 ± 4	31 ± 4
$\int \sigma_3^{1-} \frac{d\sigma}{dt} dt$	6 ± 1	6 ± 1	6 ± 2	9.6 ± 3
$\int \sigma_1^{1-} \frac{d\sigma}{dt} dt$	56 ± 6	56 ± 6	9.4 ± 3	6.6 ± 2
$\int \sigma_3^{0-} \frac{d\sigma}{dt} dt$	51 ± 6	51 ± 6	5.6 ± 2	7.3 ± 2
$\int \sigma_1^{0-} \frac{d\sigma}{dt} dt$	226 ± 12	227 ± 12	11.6 ± 3	9 ± 3
$\int \sigma_3^{1+} \frac{d\sigma}{dt} dt$	23 ± 3	23 ± 3	24.7 ± 4	20 ± 4
$\int \sigma_1^{1+} \frac{d\sigma}{dt} dt$	31 ± 4	31 ± 4	6.7 ± 2	11.1 ± 2

and is mainly associated with production of the helicity states $\lambda_\Delta = \pm\frac{1}{2}$.

B. $\pi^+p \to \omega\Delta^{++}(1236)$

Although our statistical significance for the reaction $\pi^+p \to \omega\Delta^{++}$ is poor, some observations can be made from the $\rho^{mm'}$ (Fig. 6) and $\sigma^{m\pm}$ (Fig. 10) distributions:

(a) ρ^{00} is quite large in the low-momentum-transfer region ($\rho^{00} \simeq 0.5$ at $-t \simeq 0.06$ GeV^2), and decreases to a minimum at $-t \simeq 0.15$ GeV^2. ρ_H^{00} has a value of ~0.4 at low $-t$ and gradually decreases in value as $-t$ increases.

(b) ρ^{1-1} rises from 0.0 to a value of 0.3 (0.2) in the Gottfried-Jackson (helicity) frame at $-t \simeq 0.35$ GeV^2. In both frames, this distribution is observed to be positive for almost all $-t$ values considered.

(c) For $-t \geq 0.3$ GeV^2, we note that the $M1$ ρ-exchange conditions $\rho_{33} = \frac{3}{8}$, $\rho_{3-1} = \frac{1}{8}\sqrt{3}$, and $\rho_{31} = 0$ are approximately satisfied.

(d) σ^- is found to be large for $-t \leq 0.1$ GeV^2 and decreasing with increasing momentum transfer.

(e) σ^{1+} shows a gradual increase with increasing momentum transfer to a value of 0.7 at $-t \simeq 0.35$ GeV^2. Therefore, in reaction (2), there appear two momentum transfer regions in which the relative NP and UNP contributions are different.

For $-t \leq 0.1$ GeV^2, large (small) values of σ^- and ρ^{00} (σ^{1+} and σ^{1-}) indicate the dominance of UNP exchanges producing the ω in helicity states $\lambda_\omega = 0$. At higher $-t$ values, σ^{1+} increases with increasing momentum transfer, so that at $-t \simeq 0.35$ GeV^2, the NP exchange becomes stronger

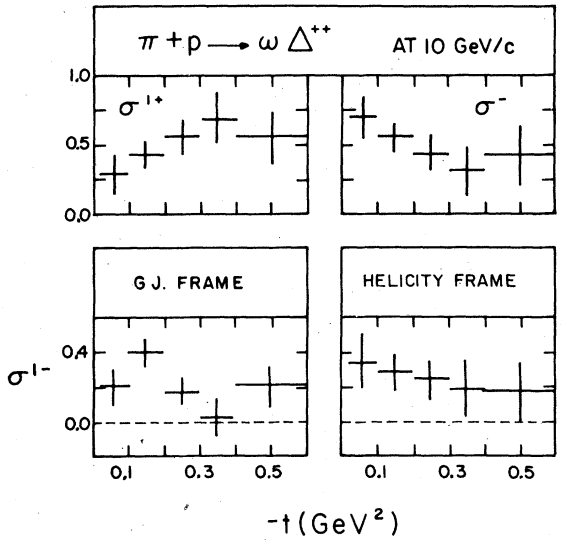

FIG. 10. Relative proportion of the natural-spin-parity exchange, σ^{1+}; the unnatural-spin-parity exchange, σ^-; the unnatural-spin-parity exchange to ω helicity ± 1, σ^{1-}.

than UNP exchange. In this $-t$ region, the UNP-exchange contribution is predominantly associated with ω production in helicity states $\lambda_\omega = \pm 1$.

From the measurable exchange cross sections summarized in Table IX, one can conclude that the UNP exchange contribution is approximately equal to that of NP exchange. Approximately 50% of the UNP exchange leads to $\lambda_\omega = 0$ helicity states production. In both frames, NP exchange leading to $\lambda_\Delta = \pm \frac{3}{2}$ helicity states is more important than that leading to $\lambda_\Delta = \pm \frac{1}{2}$.

C. Discussion

As $\rho^0(\omega)$ production by π-induced reactions can proceed only via G-parity -1 $(+1)$ exchange, the main candidates for UNP and NP exchange with isospin 1 are respectively $\pi(B)$ and $A_2(\rho)$.

For both frames, the distributions $\rho^{00}\, d\sigma/dt$ are shown in Fig. 11 for the reaction $\pi^+ p \to \rho^0 \Delta^{++}(1236)$. In both frames, $\rho^{00}\, d\sigma/dt$ is observed to have a strong forward peak which is expected from the dominant π-exchange contribution to the overall nonflip amplitudes. The fact that ρ^{00} is smaller than 1 implies, however, the need for contributions in addition to simple π exchange. Such a correction can come from, for example, cut contributions.[15] The change of slope in $\rho^{00}_H\, d\sigma/dt$ at $-t \simeq 0.4$ GeV^2 has also been observed in the reaction $\pi^- p \to \rho^0 n$.[16]

Since we expect that the π propagator, even in the presence of cuts, dominates the helicity-zero amplitudes, we performed a fit of the data for $-t < 0.5$ GeV^2 to the form

$$\rho^{00}\, d\sigma/dt = \frac{A\, e^{b|t|}}{(t - m_\pi^2)^2}.$$

The results of these fits are shown as the solid curve in Fig. 11, with

$$\rho^{00}_{GJ}\, d\sigma/dt : \begin{cases} A = 15.6 \pm 0.5\ \mu\text{b GeV}^2, \\ b = -1.4 \pm 0.3\ \text{GeV}^{-2} \end{cases}$$

and

$$\rho^{00}_H\, d\sigma/dt : \begin{cases} A = 16.4 \pm 0.5\ \mu\text{b GeV}^2, \\ b = -3.7 \pm 0.5\ \text{GeV}^{-2}. \end{cases}$$

The results indicate that neither of the distri-

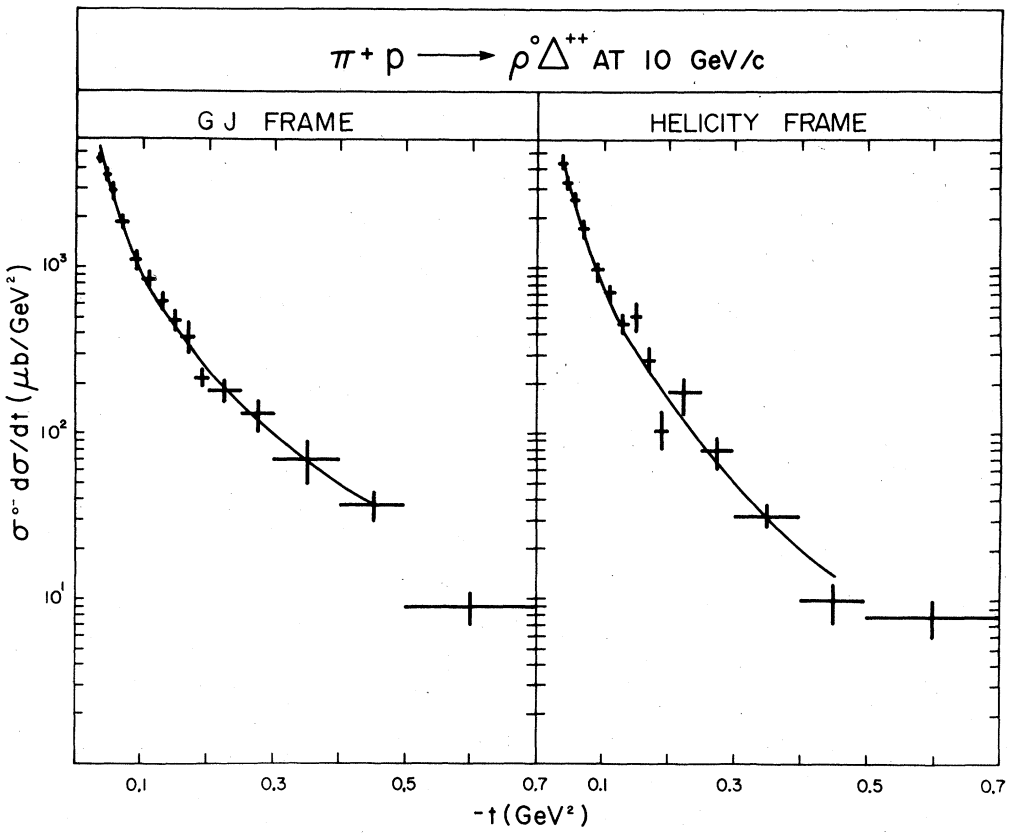

FIG. 11. The $\sigma^{0-}\, d\sigma/dt$ distribution shown as a function of momentum transfer for the reaction $\pi^+ p \to \rho^0 \Delta^{++}(1236)$ in the Gottfried-Jackson and helicity frames. The solid curves represent the results of fits to the form $A e^{b|t|}/(t - m_\pi^2)^2$.

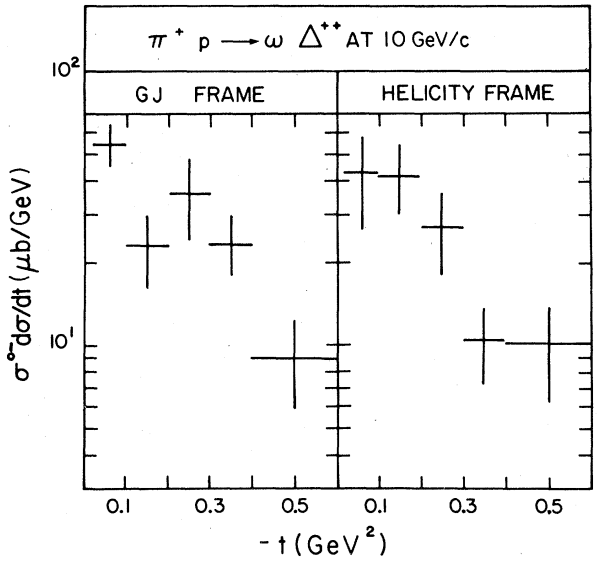

FIG. 12. The $\sigma^{0-} d\sigma/dt$ distribution shown as a function of momentum transfer for the reaction $\pi^+ p \to \omega \Delta^{++}(1236)$ in the Gottfried-Jackson and helicity frames.

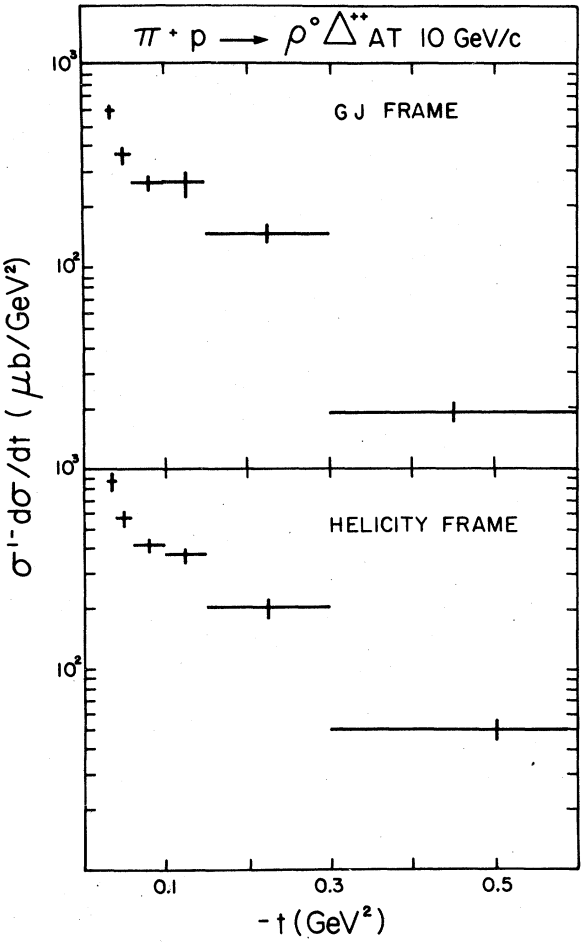

FIG. 13. The $\sigma^{1-} d\sigma/dt$ distribution shown as a function of momentum transfer for the reaction $\pi^+ p \to \rho^0 \Delta^+(1236)$ in the Gottfried-Jackson and helicity frames.

butions can be represented solely by the π propagator; an additional exponential damping factor is needed to fit the distribution away from the near forward direction. Similar behavior was noted in the reactions $\pi^- p \to \rho^0 n$ (Ref. 16) and $K^+ p \to K^{*0} \Delta^{++}(1236)$.[17]

While the Williams model[18] predicts large values of ρ^{00} as well as the correct sign of ρ^{1-1} in $\pi^+ p \to \rho^0 \Delta^{++}$ and $\pi^- p \to \rho^0 n$ (e.g. see Ref. 17), it coincides with the pure π-pole model for $\rho_H^{00} d\sigma/dt$ and hence yields values which are too low for $-t \geq 0.4$ GeV^2. Therefore we can only conclude from the excellent fits to forms which include the π propagator that the $\rho^{00} d\sigma/dt$ distributions for reaction $\pi^+ p \to \rho^0 \Delta^{++}$ have dominant contributions from π exchange.

The $\rho^{00} d\sigma/dt$ distributions for reaction (2) are shown in Fig. 12. In contrast to the $\rho^0 \Delta^{++}$ case, these distributions show no strong forward peaks and are rather flat for $-t < 0.2$ GeV^2, which implies the dominance of net helicity-flip amplitudes in the forward direction.

$\sigma^{1-} d\sigma/dt$ distributions are shown in Fig. 13 (Fig. 14) for $\pi^+ p \to \rho^0 \Delta^{++}$ ($\pi^+ p \to \omega \Delta^{++}$). In the helicity frame, this unnatural-spin-parity component receives a contribution from UNP poles plus cuts and from NP cuts, and interferences between the different contributions may make any simple description of the data impossible.

In Fig. 15 the total unnatural-spin-parity exchange contribution is compared to that of natural-spin-parity exchange for reaction (1). One expects, as in $\pi^- p \to \rho^0 n$,[16] the NP pole A_2 contribution to be small for small $-t$, so that the large value of $\sigma^{1+} d\sigma/dt$ is most naturally associated with contributions from π and A_2 cuts. The dip at $-t \simeq 0.2$ GeV^2 can be interpreted as arising from interference between the A_2 pole and A_2 and π cut terms, as is a similar structure in $\sigma^{1+} d\sigma/dt$ in $\pi^- p \to \rho^0 n$.

The corresponding distributions for the $\omega \Delta^{++}$ reaction are presented in Fig. 16. The dip in the $\sigma^{1+} d\sigma/dt$ distribution at $-t \simeq 0.2$ GeV^2, associated with the nonsense wrong-signature zero of the B-meson exchange, and reported at 16 GeV/c,[2t] is not observed in the present data. The distribution of $\sigma^{1+} d\sigma/dt$ should receive contributions from a ρ pole plus B and ρ cuts. The absence of a dip at $-t \simeq 0.6$ GeV^2, due to the wrong-signature nonsense zero of the ρ trajectory, may be explained by the presence of $(\rho + B)$-cut contributions.[15]

Moreover, if the cross section for reaction (1)

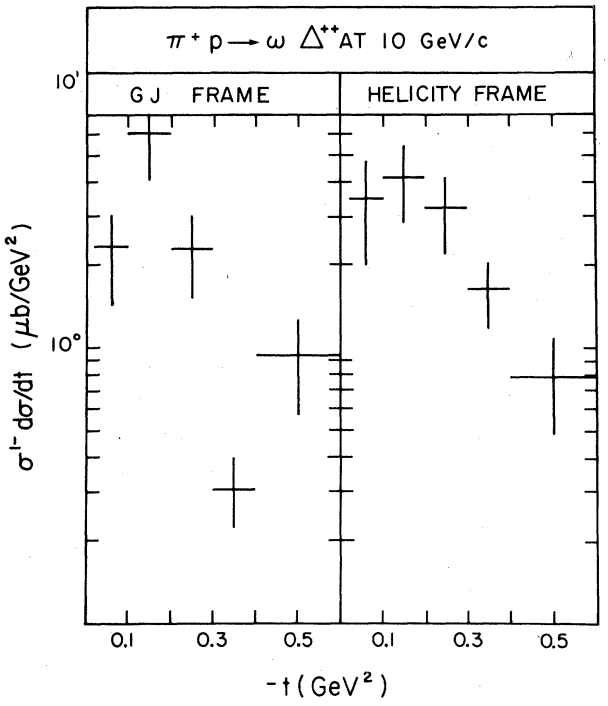

FIG. 14. The $\sigma^{1-} d\sigma/dt$ distribution shown as a function of momentum transfer for the reaction $\pi^+ p \to \omega\Delta^{++}(1236)$ in the Gottfried-Jackson and helicity frames.

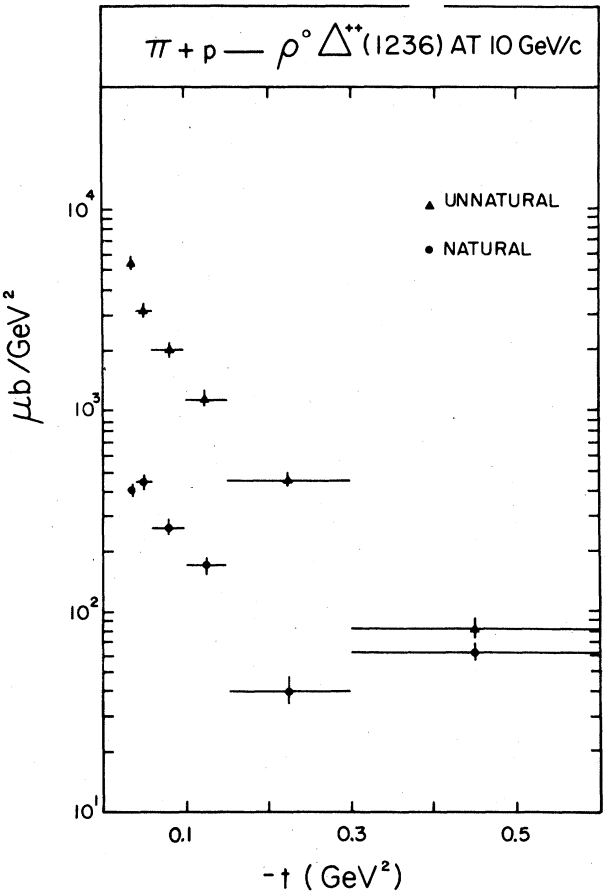

FIG. 15. The contributions due to unnatural-spin-parity exchanges and to natural-spin-parity exchanges as functions of momentum transfer for the reaction $\pi^+ p \to \rho^0\Delta^{++}(1236)$.

[(2)] were dominated by π and A_2 (B and ρ) exchanges, the fraction of NP exchange, σ^{1+}, would be expected to increase with energy since the $A_2(\rho)$ trajectory lies higher than the corresponding π (B) trajectory. However, when we compare our cross sections (given in Table IX) with those obtained at 16 GeV/c,[1w] for the reaction (1), we note that the NP-exchange contribution decreases with energy, while the UNP-exchange contribution increases. For reaction (2), strong energy dependence between 10 GeV/c and 16 GeV/c (Ref. 2t) is not observed.

We conclude then that our data cannot be described by only single pole exchanges. Non-pole-like terms, (referred to as cut contributions in the text), such as absorptive corrections, are necessary to describe all the observed structures.

VIII. VECTOR-MESON POLARIZATION CONE

As discussed by Doncel *et al.*[19] an alternative description of the production mechanism may be given by the investigation of polarization matrices. Assuming that a single Reggeized particle exchange with factorizable residues dominates the production amplitudes, the exchanged parity and degree of polarization are traced by a path in a two-dimensional projection of the polarization domain.

The vector-meson-polarization properties of reactions (1) and (2) are studied by expanding the normalized angular distribution in terms of a set of real parameters r_M^2:

$$W(\theta_V, \phi_V) = \frac{1}{4\pi}\left\{1 - 2r_0^2\left(\frac{4\pi}{5}\right)^{1/2} Y_0^2 - 4\left(\frac{2\pi}{5}\right)^{1/2}[r_2^2 \mathrm{Re}(Y_2^2) + r_{-2}^2 \mathrm{Im}(Y_2^2)] + 4\left(\frac{2\pi}{5}\right)^{1/2}[r_1^2 \mathrm{Re}(Y_1^2) + r_{-1}^2 \mathrm{Im}(Y_1^2)]\right\} \quad (22)$$

where the r_M^L are related to the multipole parameters t_M^L by

$$r_{\pm M}^L = (-1)^M \left(\frac{2L+1}{j}\right)^{1/2} \begin{pmatrix}\mathrm{Re}\\ \mathrm{Im}\end{pmatrix} t_M^L,$$

$$r_0^L = \left(\frac{2L+1}{j}\right)^{1/2} t_0^L.$$

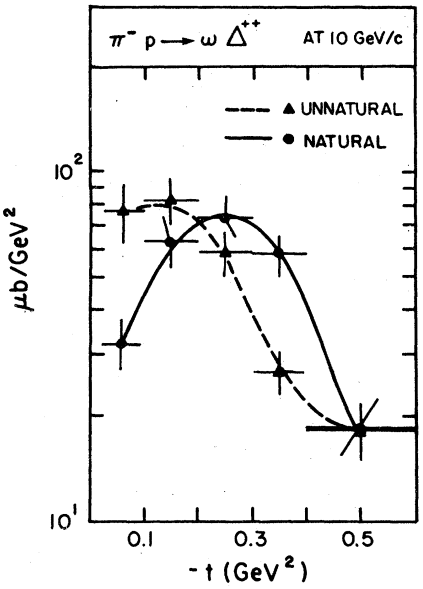

FIG. 16. The contributions due to unnatural-spin-parity exchanges and to natural-spin-parity exchanges as functions of momentum transfer for the reaction $\pi^+ p \rightarrow \omega \Delta^{++}$. The full and dashed curve are shown only to guide the eye.

An additional superscript T (as in ${}^T r^L_{\pm M}$) will indicate that our results are presented in transversity frames, where the r^L_M with odd M vanish.[20]

In the transverse Gottfried-Jackson (transverse helicity) frame, the y axis is taken along the direction of the incoming particle (along the direction of the decaying system).

An orthonormal coordinate system is defined by the nonvanishing parameters ${}^T r^2_0$, ${}^T r^2_2$, ${}^T r^2_{-2}$; in this space the domain of polarization of the vector meson is contained inside a cone whose axis lies along ${}^T r^2_0$. With the unpolarized state at the origin, the apex of the cone reaches ${}^T r^2_0 = -1$ and the base, of radius $\frac{1}{2}\sqrt{3}$, is at ${}^T r^2_0 = \frac{1}{2}$. Each internal point of the cone represents a state of polarization and the boundary corresponds to a positivity condition. More details may be found in Ref. 19.

Projections of the ρ^0 polarization domain are presented in Fig. 17 for both transversity frames, where each point represents an average over a Δt interval. In each frame the data points are close to the rim of the cone for low-momentum transfer, indicating polarization in the reaction plane and unnatural-parity exchange. As $-t$ in-

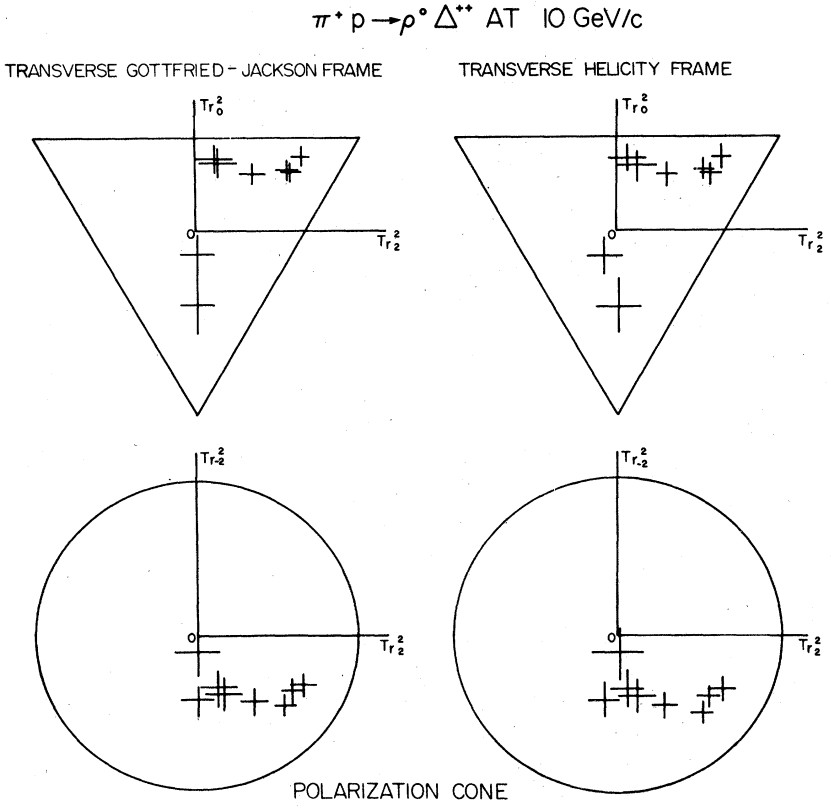

FIG. 17. Side and top projections of the ρ^0 polarization domain in the transverse Gottfried-Jackson and transverse helicity frames.

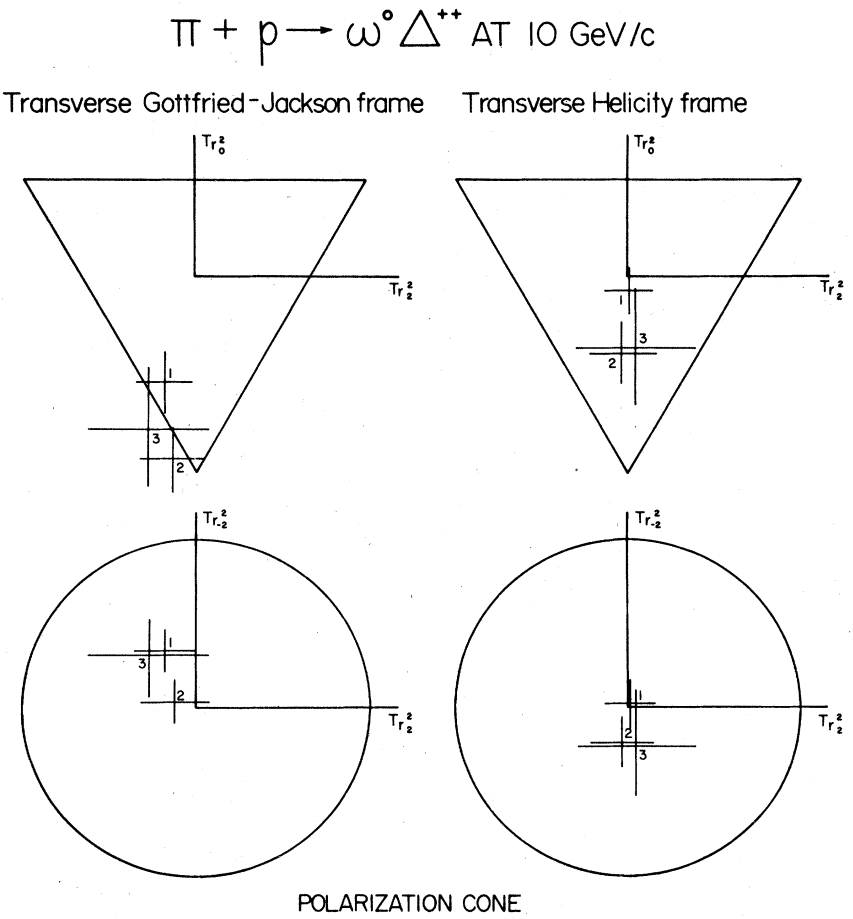

FIG. 18. Side and top projections of the ω^0 polarization domain in the transverse Gottfried-Jackson and helicity frames. The numbers adjacent to the data points identify the Δt interval.

creases, the points trace a curve through the cone toward the axis and approach the apex, where the polarization is normal to the reaction plane and the exchanged particle has natural parity.

A different picture emerges from the projections of the ω polarization domain in Fig. 18. There is a large degree of polarization normal to the reaction plane revealing the dominance of natural-parity ρ exchange.

These pictures are consistent with the results of density-matrix analyses presented previously. Similar projections (not shown) of the Δ^{++} polarization spherical domain are also in agreement with the behavior exhibited by the $\rho_{mm'}$.

Similar results have been obtained at 13.1 GeV/c.[17]

IX. EQUAL-PHASE HYPOTHESIS

Several models of quasi-two-body reactions assume that all helicity amplitudes in a given reaction have the same phase. This dynamical assumption can be directly tested in certain cases.

The tests derived by Donohue and Plaut[21] to check the equal-phase hypothesis are exact mathematical consequences of the hypothesis itself. The validity of this assumption requires that particular bilinear combinations of the even-rank statistical tensors must vanish. Using the notation of Ref. 21, these requirements are expressed as $C_L^S = 0$ for $S = 0, 2, 4$ and $0 \leq L \leq S$.

The quantities C_L^S are defined by

$$C_L^S = \sum_{\substack{L_1, L_1'=0 \\ \text{even}}}' G(L_1, L_1', S) H(S, L, L_1, L_1'), \qquad (23)$$

where the $G(L_1, L_1', S)$ are numerical factors (for details see Ref. 21). The $H(S, L, L_1, L_1')$ are explicitly given by

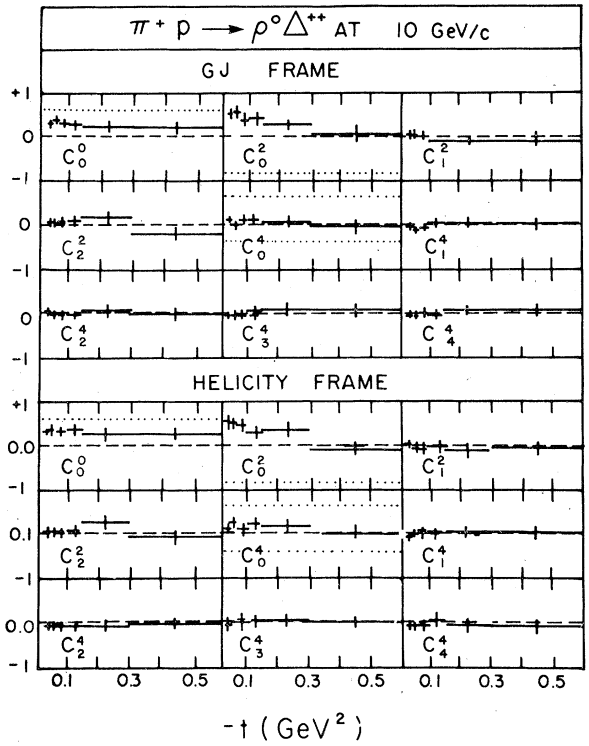

FIG. 19. Values of the quantities C_L^S evaluated in the Gottfried-Jackson and helicity frames for the reaction $\pi^+ p \to \rho^0 \Delta^{++}$ (1236) as functions of the momentum transfer. The dotted lines are the extreme values allowed.

$$H(S,L,L_1,L_1') = \sum_{\substack{-L_1 \le M_1 \le L_1 \\ -L_1' \le M_1' \le L_1'}} (-1)^{M_1'} \langle L_1, M_1; L_1', -M_1', | S, L \rangle \times \left(t^{L_1 0}_{M_1 0}\, t^{L_1' 0}_{M_1' 0} - 5 \sum_{-2 \le M_2 \le 2} t^{L_1 2}_{M_1 M_2}\, t^{L_1' 2}_{M_1 M_2} \right),$$

where the $t^{LL'}_{MM'}$ are simply related to $T^{LL'}_{MM'}$.[21] The derivation of the tests is based on the assumption that the quantization axis is in the production plane.

The nine quantities C_L^S evaluated in the Gottfried-Jackson and helicity frames are presented in Fig. 19 as functions of $-t$ for reaction (1). The extreme values allowed for $C_0^0(0, \frac{3}{5})$, $C_0^2(-\frac{6}{7}, \frac{12}{7})$, and $C_0^4(-\frac{12}{35}, \frac{24}{35})$ (the upper bounds on C_0^2 and C_0^4 are believed, but are not proved to be true[21]) are shown as dotted horizontal lines.

One observes that (i) deviations from zero are seen in all $-t$ intervals for C_0^S; (ii) the quantities C_0^0, C_0^2, and C_0^4 are within the bounds given. In particular, the quantity C_0^0 is non-negative as required; (iii) the C_L^S with $L \neq 0$, which have to be zero in the forward direction, are indeed small

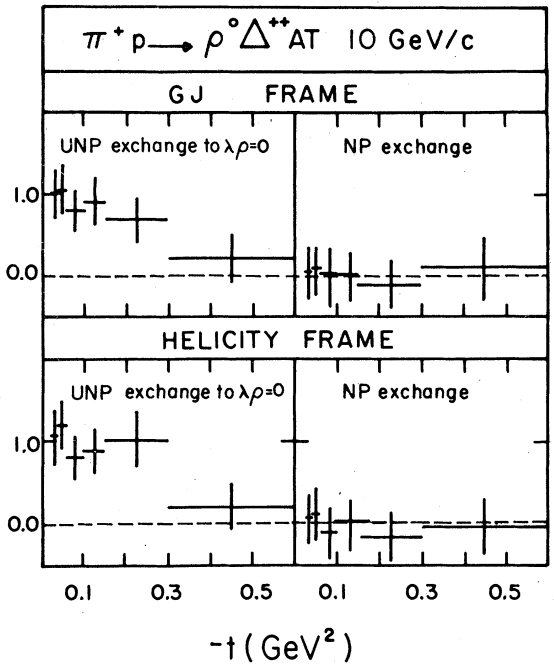

FIG. 20. Values of the linear combinations of C_L^S which represent the conditions for unnatural spin-parity (UNP) exchange amplitudes leading to $\lambda_\rho = 0$ and for natural-spin-parity (NP) exchange amplitudes to be in phase, shown as functions of the momentum transfer in the Gottfried-Jackson and helicity frames.

in the first $-t$ interval.

A more restricted form of the equal-phase hypothesis is related to amplitudes receiving only contributions from either natural- or unnatural-spin-parity exchange leading to ρ^0-helicity zero states. For NP exchange the condition is[21]

$$C_0^0 - \tfrac{1}{2} C_0^2 - \tfrac{1}{2}\sqrt{6}\, C_2^2 + \tfrac{3}{8} C_0^4 + \tfrac{1}{4}\sqrt{10}\, C_2^4 + \tfrac{1}{8}\sqrt{70}\, C_4^4 = 0. \quad (24)$$

The test for UNP exchange with $\lambda_\rho = 0$ is

$$C_0^0 + C_0^2 + C_0^4 = 0. \quad (25)$$

In Fig. 20 are shown the linear combinations (24) and (25) as functions of $-t$ for reaction (1).

Although the linear combination of C_L^S which measures the phase difference amoung natural-parity amplitudes is consistent with zero in the range considered, the amplitudes for unnatural-parity exchange leading to $\lambda_\rho = 0$ are not in phase at small momentum transfer. Thus, in agreement with results at 13.1 (Ref. 1v) and 16.0 (Ref. 1w) GeV/c, we conclude that the equal-phase hypothesis is not valid for the reaction $\pi^+ p \to \rho^0 \Delta^{++}$.

As stated previously the forward peak in $\rho^{00}\, d\sigma/dt$ indicates the dominance of net nonflip amplitudes with $\lambda_\rho = 0$. Therefore, denoting helicity

amplitudes by $f_{\lambda_V \lambda_\Delta \lambda_N}$, one expects the $f_{0(1/2)(1/2)}$ helicity amplitude to dominate $\rho\Delta$ production as $-t \to 0$ and so determine the relative amounts of the other two net helicity-flip amplitudes as $-t \to 0$. Using our previously determined values of the density matrix elements, we find

$$|f_{1(1/2)(-1/2)}/f_{1(3/2)(1/2)}| = \left(\frac{1-\rho^{00}}{2\rho^{33}} - 1\right)^{1/2} \simeq 0.0,$$

$$|f_{1(3/2)(1/2)}/f_{0(1/2)(1/2)}| = \left(\frac{2\rho^{33}}{\rho^{00}}\right)^{1/2} \simeq 0.61 \pm 0.09,$$

$$\phi(f_{1(3/2)(1/2)}) - \phi(f_{0(1/2)(1/2)}) = \cos^{-1}[T^{22}_{11}/(\rho_{33}\rho^{00})^{1/2}] \simeq 103 \pm 20^\circ.$$

We observe that the $f_{1(3/2)(1/2)}$ helicity amplitude is nonzero as $-t \to 0$ and substantially out of phase with the dominant amplitude $f_{0(1/2)(1/2)}$. Similar values within errors have been obtained at 3.7 (Ref. 1i) and 13.1 GeV/c.[1v]

Donohue *et al.*[12] have shown that if all amplitudes were in phase, then the positivity condition on joint spin-density matrix elements, discussed in Sec. VI, would be saturated.

These authors then propose that a combination of dynamical and statistical effects leads to the observed experimental fact that almost all experimental points lie just "outside" the boundary of the positivity domain. Some unknown dynamical effect is hypothesized to cause the points to fall near the domian boundary, and statistical fluctuations then lead to the appearance of many of the points in the exterior of the domain. Such a dynamical mechanism might also cause some of the major amplitudes to have small phase differences.

X. TEST OF FACTORIZATION

In the Regge model, the residue function factorizes, i.e., the t-channel helicity amplitude is written as

$$f^t_{\lambda_c \lambda_d, \lambda_a \lambda_b} = \gamma_{\lambda_a \lambda_c}\ (\text{upper vertex}) \times \gamma_{\lambda_b \lambda_d}\ (\text{lower vertex}) F(s,t), \quad (26)$$

where $F(s,t)$ is helicity independent.

In the presence of Regge cuts, simple factorization would not be expected to hold. However, as Regge cuts are known to affect the phase of Regge poles in a helicity-dependent way, a test of factorization is expected to be most favorable in cases where only the moduli, and not the phases, of $\gamma_{\lambda_a \lambda_c}$ and $\gamma_{\lambda_b \lambda_d}$ are involved.[22]

Such a test is

$$\frac{d\sigma/dt(\pi^- p \to \eta n)}{d\sigma/dt(\pi^+ p \to \eta \Delta^{++})} = \frac{\sigma^{1+} d\sigma/dt(\pi^- p \to \rho^0 n)}{\sigma^{1+} d\sigma/dt(\pi^+ p \to \rho \Delta^{++})}, \quad (27)$$

where all observables involve (asymptotically) A_2-exchange quantum numbers. The equality (27) is expected due to a cancellation of the upper (meson-meson) vertex in the two ratios. Figure 21 shows the test of Eq. (27) at $p_{1ab} \simeq 10$ GeV/c. The $\pi^+ p$ data are taken from this experiment. For the $\pi^- p \to \eta n$ we use the data of Wahlig and Mannelli[23] at 10 GeV/c (corrected for unseen η decay modes), while for $\pi^- p \to \rho^0 n$ we have used the data at 15 GeV/c (Ref. 24) scaled to 10 GeV/c by an expression of the form of Eq. (8), with $n = 1.89$.[25] Although, for both $\pi^- p \to \rho^0 n$ and $\pi^+ p \to \rho^0 \Delta^{++}$ reactions, the natural-parity contribution is expected to be small in the low $-t$ region, (as previously noted) the test does not show a strong deviation from factorization.

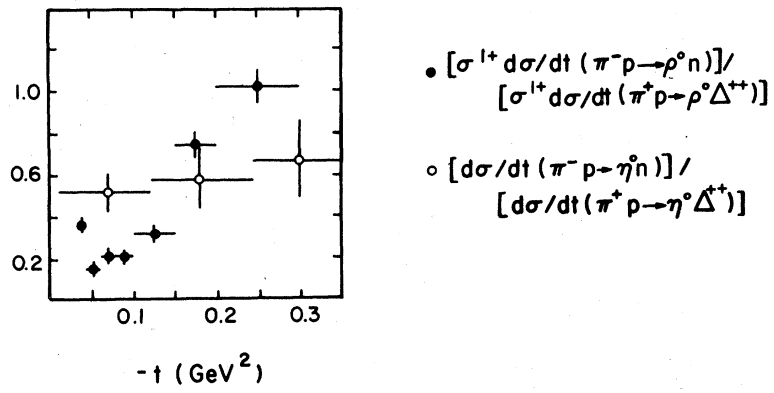

FIG. 21. Test of the factorization relation for A_2 exchange as a function of momentum transfer.

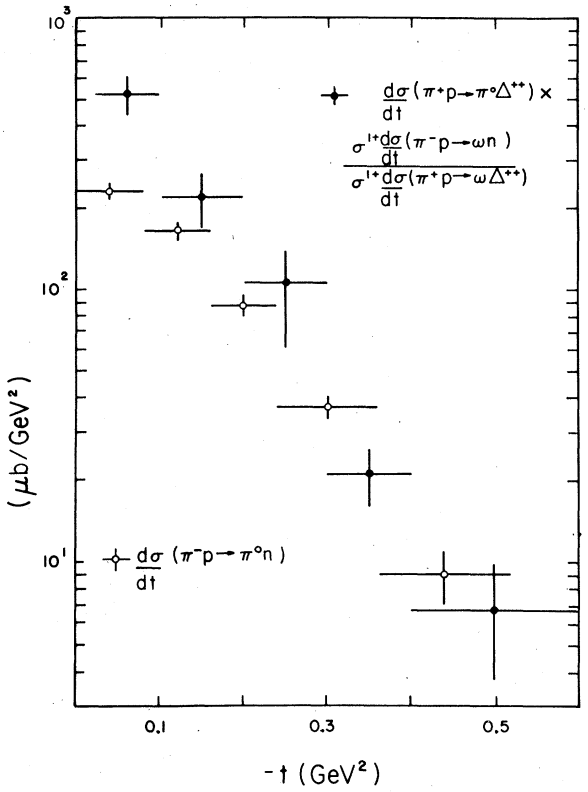

FIG. 22. Test of the factorization relation for ρ exchange as a function of momentum transfer.

The predicted equality

$$\frac{d\sigma/dt(\pi^- p\to\pi^0 n)}{d\sigma/dt(\pi^+ p\to\pi^0\Delta^{++})}=\frac{\sigma^{1+}d\sigma/dt(\pi^- p\to\omega n)}{\sigma^{1+}d\sigma/dt(\pi^+ p\to\omega\Delta^{++})} \tag{28}$$

provides an analogous test involving ρ-exchange quantum numbers. The result is presented in Fig. 22. We have used $\pi^- p\to\pi^0 n$ at 10 GeV/c,[23] $\pi^+ p\to\pi^0\Delta^{++}$ at 8 GeV/c (Ref. 1s) scaled to 10 GeV/c using the form of Eq. (8) with $n=1.24$.[25] For $\pi^- p\to\omega n$, we used data at 12 GeV/c,[26] scaled using the form of Eq. (8) with $n=2.41$.[26] Within errors, this test is again successful, although the two quantities entering the ratio on the right-hand side of Eq. (28) do not show the dip at $-t\simeq 0.6$ GeV^2 expected from a pure ρ Regge exchange, and thus have presumably appreciable Regge cut contributions.

Similar tests are possible for the unnatural-parity-exchange contribution. In this case a predicted equality is

$$\frac{\sigma^{1-}}{\sigma^{0-}}(\pi^- p\to\omega n)=\frac{\sigma^{1-}}{\sigma^{0-}}(\pi^+ p\to\omega\Delta^{++}), \tag{29}$$

which involves mainly B-quantum-numbers exchange (ignoring π exchange due to electromagnetic ρ-ω mixing). In this case the lowest (baryon-

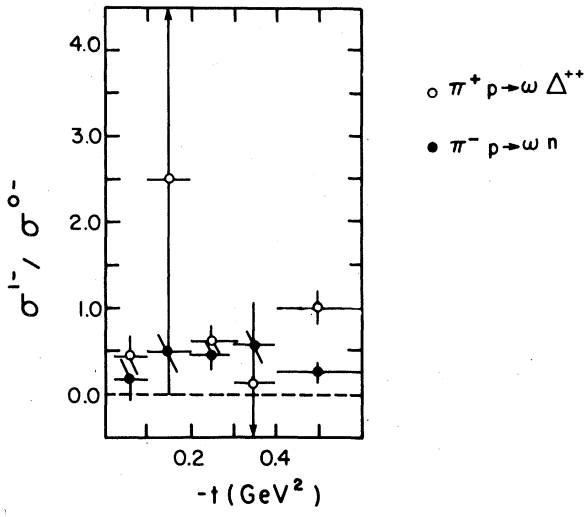

FIG. 23. Test of the factorization relation for B exchange as a function of momentum transfer.

baryon) vertex is expected to cancel in the ratios. This test has the advantage of being independent of energy and of the absolute normalization of the data. Again, this test is certainly nontrivial since it explicitly involves amplitudes with zero-helicity flip, which are expected to have Regge-cut contributions. The test (29) is presented in Fig. 23 and is once again successful within errors.

Finally, one does not expect[27] factorization to work for the analogous relation to (29) involving π exchange:

$$\frac{\sigma^{1-}}{\sigma^{0-}}(\pi^- p\to\rho^0 n)=\frac{\sigma^{1-}}{\sigma^{0-}}(\pi^+ p\to\rho^0\Delta^{++}). \tag{30}$$

Both reactions receive contributions of nonfactorizing cuts. In fact, in Fig. 24, the data are sur-

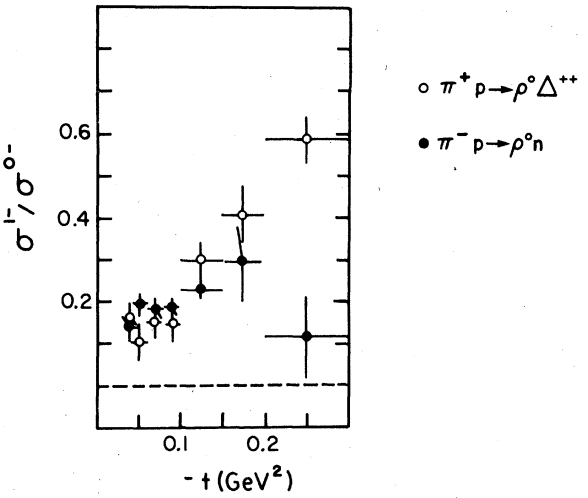

FIG. 24. Test of the factorization relation for π exchange as a function of momentum transfer.

prisingly close together and may indicate a similar behavior of the amplitudes in $\pi^- p \to \rho^0 n$ and $\pi^+ p \to \rho^0 \Delta^{++}$.

Similar successful tests were reported earlier[22,26] and may indicate (although errors are sometimes large) that Regge cuts exhibit some factorizing properties,

XI. $\rho\Delta$, $\omega\Delta$, $K^*\Delta$, AND SU(3)

Reactions (1) and (2) can be related to

$$K^+ p \to K^{*0}(890)\Delta^{++}(1236), \tag{31}$$

$$K^- n \to \bar{K}^{*0}(890)\Delta^-(1236), \tag{32}$$

and

$$K^- p \to \bar{K}^{*0}(890)\Delta^0(1236) \tag{33}$$

through the assumption of t-channel exchange with SU(3) coupling at the meson vertex. The further assumption of ideal mixing of ω and ϕ enables the amplitudes of these processes to be expressed in terms of two amplitudes A_+ and A_- corresponding, respectively, to specific helicity amplitudes with a $G=+1$ and $G=-1$ exchange contribution:

$$A(\rho^0\Delta^{++}) = \sqrt{2}\, A_-, \tag{34a}$$

$$A(\omega\Delta^{++}) = \sqrt{2}\, A_+, \tag{34b}$$

$$A(K^{*0}\Delta^{++}) = A_+ + A_-, \tag{34c}$$

$$A(\bar{K}^{*0}\Delta^-) = A_+ - A_-, \tag{34d}$$

$$A(\bar{K}^{*0}\Delta^0) = 1/\sqrt{3}\, A(\bar{K}^{*0}\Delta^-). \tag{34e}$$

Relations (34) provide the following sum rule between the observables of reaction (1), (2), (31), and (32):

$$\rho_{mm'} \frac{d\sigma}{dt}(\rho^0\Delta^{++}) + \rho_{mm'} \frac{d\sigma}{dt}(\omega\Delta^{++}) = \rho_{mm'} \frac{d\sigma}{dt}(\bar{K}^{*0}\Delta^{++}) + \rho_{mm'} \frac{d\sigma}{dt}(\bar{K}^{*0}\Delta^-). \tag{35}$$

The SU(3) factorization is a weaker assumption than the one expressed in Eq. (26) of the preceding section. Since SU(3) relates amplitudes of different reactions for a fixed helicity configuration, the amplitude may be written as

$$f_{\{\lambda_i\}}(s,t) = \gamma_{\lambda_a \lambda_c}(\text{upper vertex}) \times \gamma_{\lambda_b \lambda_d}(\text{lower vertex}) \bar{f}_{\{\lambda_i\}}(s,t), \tag{36}$$

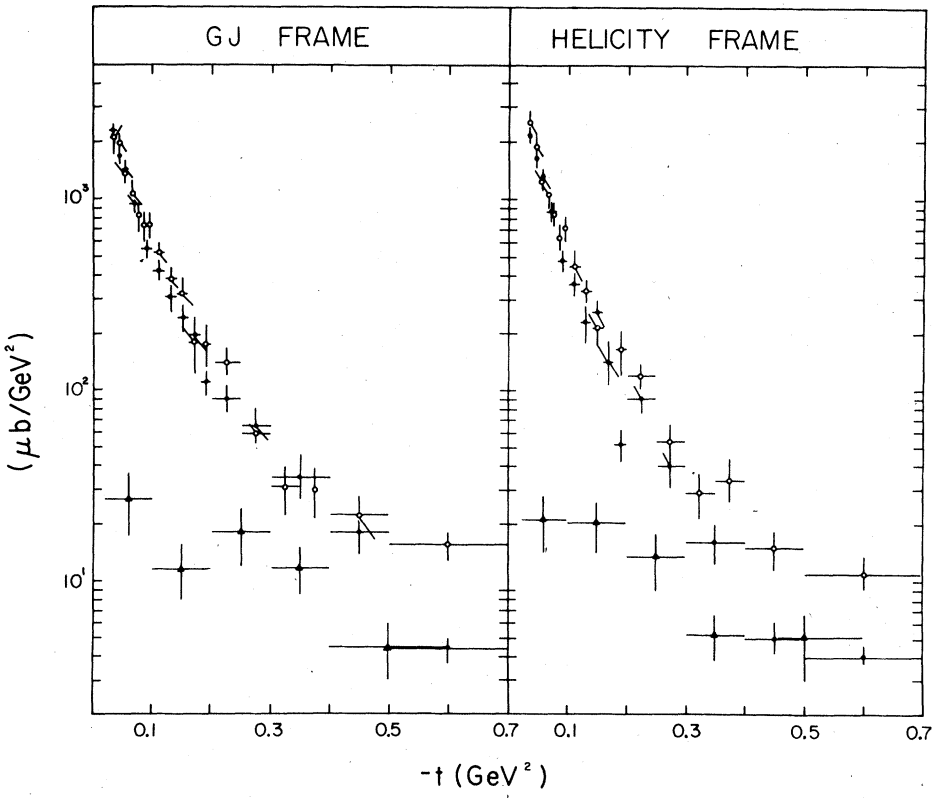

FIG. 25. The unnatural-parity helicity zero projections as functions of $-t$, in the Gottfried-Jackson and helicity frames. For $\rho^0\Delta^{++}$ (●) and $\omega\Delta^{++}$ (▲) $\frac{1}{2}\rho^{00} d\sigma/dt$ is shown while for $K^{*0}\Delta^{++}$ (○) $\rho^{00} d\sigma/dt$ is presented.

where $\bar{f}_{\{\lambda_i\}}$ have to be equal for all processes participating in the SU(3) relation, but may depend on helicities. SU(3) factorization (36) is not expected to hold in the presence of Regge cuts.[22]

The aim of the following section is to exploit Eq. (35) to learn more about the nature of the exchange mechanism in the processes (1), (2), (31), and (32).

A. Comparison of the production mechanism

The data for reaction (31) are those of the "10-GeV/c group" of Ref. 17; all of their quoted cross sections have been multiplied by a factor of 1.5 to take into account the unseen decay mode $K^{*0} \to K^0\pi^0$. A multiplicative factor of 0.96 has also been introduced to correspond to the region $M - 4\Gamma(V^0) \leq M(V^0) \leq M + 4\Gamma(V^0)$, where $M(V^0)$ [$\Gamma(V^0)$] is the mass (width) of the vector meson [Ref. 17 used $\pm 6\,\Gamma(V^0)$]. In both experiments, the same ($p\pi^+$) mass interval was used.

In Fig. 25 the UNP contributions to vector-meson helicity-zero states are presented: The $\frac{1}{2}\rho^{00}d\sigma/dt$ distributions for $\rho^0\Delta^{++}$ (closed circles) and $\omega\Delta^{++}$(triangles) are compared to the $\rho^{00}d\sigma/dt$ for $K^{*0}\Delta^{++}$ (open circles) as functions of momentum transfer. At small $-t$, in both frames, we observe that

$$\tfrac{1}{2}\rho^{00}d\sigma/dt(\rho^0\Delta^{++}) \gg \tfrac{1}{2}\rho^{00}d\sigma/dt(\omega\Delta^{++}).$$

According to (34) this implies that the $G=-1$ exchange contribution observed in $\rho^0\Delta^{++}$ (e.g., π exchange) dominates the $K^{*0}\Delta^{++}$ reaction for small momentum tranasfer. Thus SU(3) would predict

$$\tfrac{1}{2}\rho^{00}d\sigma/dt(\rho^0\Delta^{++}) \simeq \rho^{00}d\sigma/dt(K^{*0}\Delta^{++}) \qquad (37)$$

in the small $-t$ region; this relationship is seen to be satisfied in Fig. 25 for both frames. We stress that no relative normalization of the two experiments was necessary to obtain these results. Similar studies were performed at $p_{\rm lab} \simeq 7.0$ GeV/c (Ref. 15) and at $p_{\rm lab} \simeq 5.5$ GeV/c.[28] The former also verified the equality (37); however, the latter, using data obtained from two different experimen-

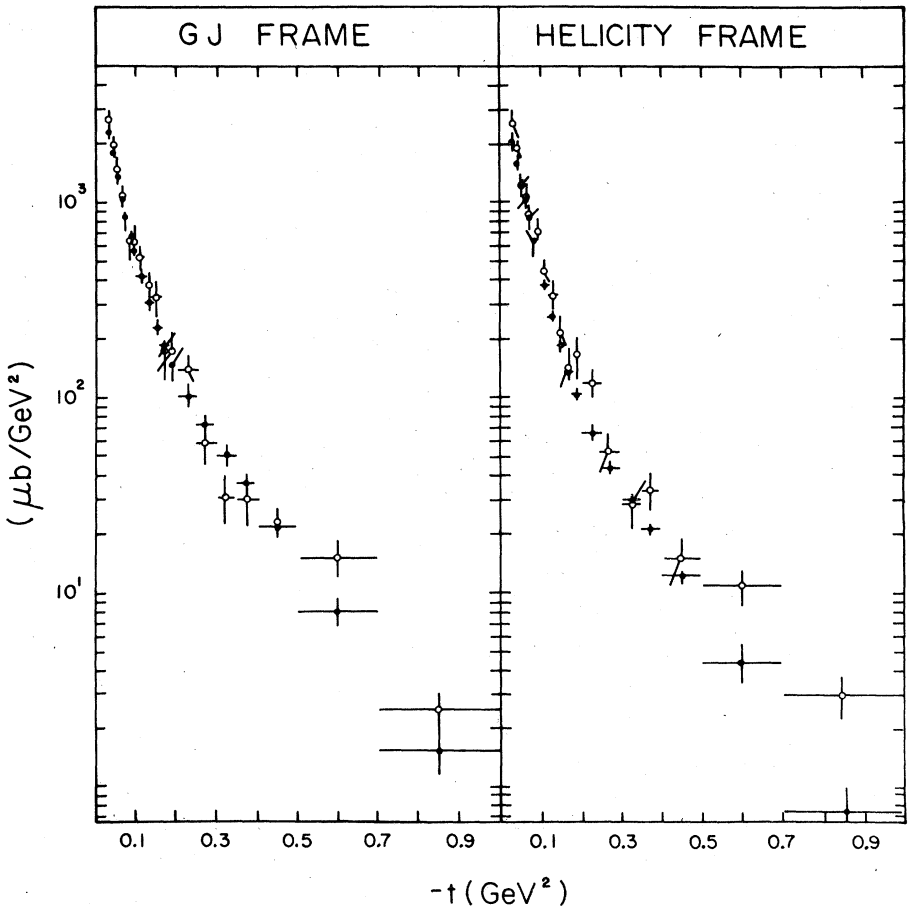

FIG. 26. $\rho^{00}d\sigma/dt$ ($K^{*0}\Delta^{++}$) (○) and $\frac{1}{2}[\rho^{00}d\sigma/dt\,(\rho^0\Delta^{++}) + \rho^{00}d\sigma/dt$ ($\omega\Delta^{++}$)] (●) as functions of momentum transfer in the Gottfried-Jackson and helicity frames.

tal techniques, required a large relative normalization factor between the values of the cross sections for $\rho^0\Delta^{++}$ and $K^{*0}\Delta^{++}$.

In the large-momentum-transfer region, one observes

$$\rho^{00}d\sigma/dt(\omega\Delta^{++}) \simeq \rho^{00}d\sigma/dt(\rho\Delta^{++}),$$

which implies [see Eq. (34)] that the $G=+1$ exchange contribution to helicity-zero states becomes comparable to that of the $G=-1$ contribution at these larger $-t$ values. In Fig. 26 the distributions $\rho^{00}d\sigma/dt$ $(K^{*0}\Delta^{++})$ and our extrapolated data, $\frac{1}{2}[\rho^{00}d\sigma/dt(\rho^0\Delta^{++}) + \rho^{00}d\sigma/dt(\omega\Delta^{++})]$, are compared in both frames: Essentially for all values of momentum transfer, we observe that

$$\rho^{00}d\sigma/dt(K^{*0}\Delta^{++}) \simeq \tfrac{1}{2}\rho^{00}d\sigma/dt(\rho^0\Delta^{++}) + \tfrac{1}{2}\rho^{00}d\sigma/dt(\omega\Delta^{++})$$

holds in both frames as these considerations suggest. This equality and the sum rule (35) then predict that

$$\rho^{00}d\sigma/dt(K^{*0}\Delta^{++}) \simeq \rho^{00}d\sigma/dt(\bar{K}^{*0}\Delta^{-}). \quad (38)$$

If this equality were exact, it would imply that the $G=-1$ (π-like) and $G=+1$ (B-like) exchanges must be $\pm\frac{1}{2}\pi$ out of phase. Such a circumstance would occur, for example, if weakly exchange-degenerate Regge poles dominated these components.

B. SU(3) predictions for $K^-n \to \bar{K}^{*0}\Delta^-$

Since there are no corresponding data for the reaction (32) near 10 GeV/c, we use the SU(3) sum rule (35) and the extrapolated $\rho\Delta^{++}$, $\omega\Delta^{++}$, and $K^{*0}\Delta^{++}$ data to predict observables for $K^-n \to \bar{K}^{*0}\Delta^-$. The predicted $d\sigma/dt$ for this reaction is shown in Fig. 27 (closed circles) and compared with the corresponding distribution for the line reversed reaction $K^+p \to K^{*0}\Delta^{++}$.

Duality arguments for a pair of line-reversal reactions demand that the exchange of a pair of exchange-degenerate Regge poles produce a real amplitude in $K^+p \to K^{*0}\Delta^{++}$ and a rotating phase $(e^{-i\pi\alpha(t)})$ in $K^-n \to \bar{K}^{*0}\Delta^-$. Therefore, the assumption of line-reversal symmetry would predict the equality of the differential cross section for these two processes. In fact, one observes in Fig. 27, that the cross section of the "real" process, $K^+p \to K^{*0}\Delta^{++}$ (open circles), is predicted to be smaller than that of the "rotating" process, $K^-n \to \bar{K}^{*0}\Delta^-$. The breaking of the line-reversal symmetry, observed in many other reactions (see, for instance, Ref. 22), is then excellently reproduced by the SU(3) sum rule.

A fit to $d\sigma/dt(\bar{K}^{*0}\Delta^-)$ with the sum of two exponentials

$$d\sigma/dt \propto \exp(At) + C\exp(Bt)$$

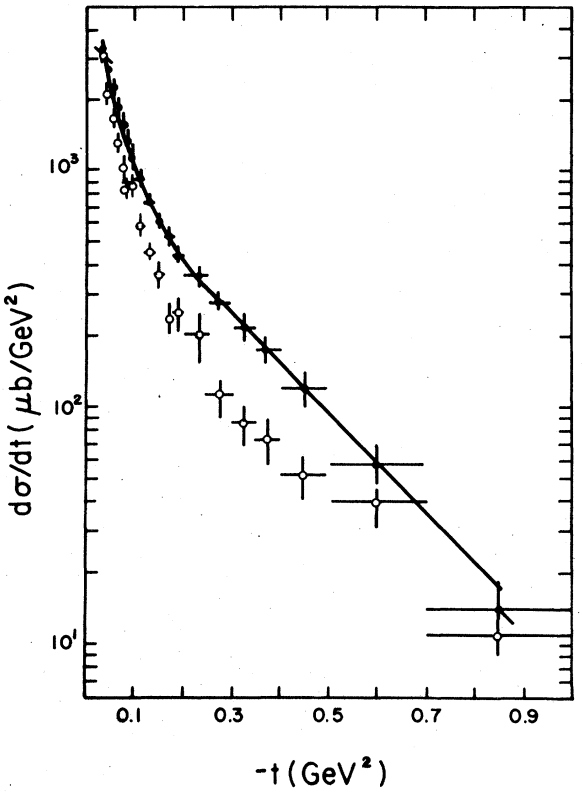

FIG. 27. SU(3)-predicted differential cross section $d\sigma/dt$ $(K^-n \to \bar{K}^{*0}\Delta^-)$ (●). The error bars correspond to an estimate of the errors of SU(3) prediction as deduced from the errors of the extrapolations of the quoted data on $K^+p \to K^{*0}\Delta^{++}$, $\pi^+p \to \rho^0\Delta^{++}$, and $\pi^+p \to \omega\Delta^{++}$. The solid curve represents the fit with the expression $d\sigma/dt \propto \exp(At) + C\exp(Bt)$. The differential cross section $d\sigma/dt$ $(K^{*0}\Delta^{++})$ (○) is also shown for comparison (Ref. 17).

yields $A = (26.7 \pm 1.5)$ GeV^{-2} and $B = (4.7 \pm 0.19)$ GeV^{-2} (the fit is shown by the solid curve in Fig. 27). The agreement between the values and those obtained in a similar fit to the corresponding distribution of $K^-p \to \bar{K}^{*0}\Delta^0$ at 10 GeV/c (Ref. 29) implies that the shape of $d\sigma/dt$ $(K^-p \to \bar{K}^{*0}\Delta^0)$ [or $d\sigma/dt$ $(K^-n \to \bar{K}^{*0}\Delta^-)$, via Eq. (34e)] is well produced by SU(3).

In Fig. 28 a comparison of the total unnatural-parity exchange contribution ($\sigma^- d\sigma/dt$) is presented for reactions (31) and (32). We observe that

$$A_{\mathrm{UNP}}(K^{*0}\Delta^{++}) \simeq A_{\mathrm{UNP}}(\bar{K}^{*0}\Delta^-). \quad (39)$$

Therefore the previously observed difference in cross section is due mainly to the natural-parity-exchange contribution:

$$\sigma^{1+}d\sigma/dt(K^{*0}\Delta^{++}) < \sigma^{1+}d\sigma/dt(\bar{K}^{*0}\Delta^-).$$

This situation would be expected from a simple absorbed exchange-degenerate (ρ, A_2) Regge model,

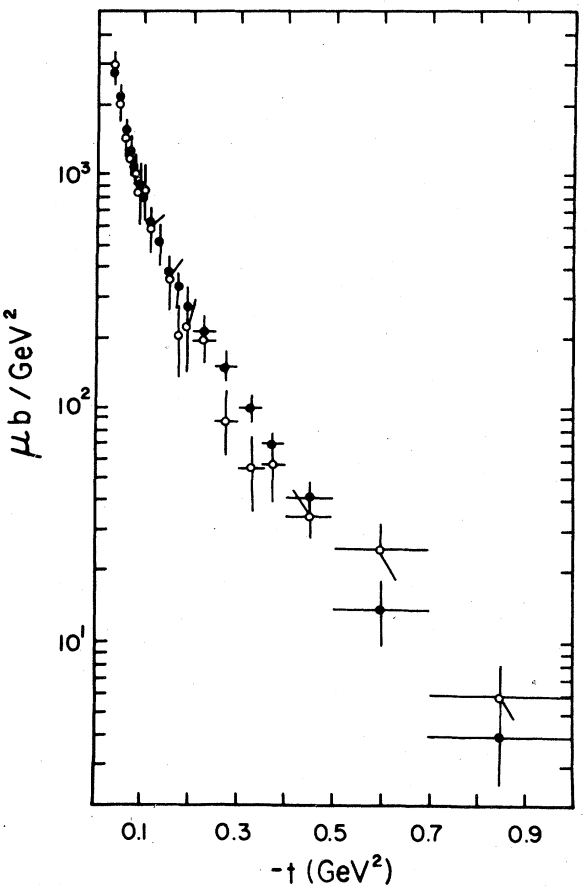

FIG. 28. The SU(3)-predicted unnatural-parity-exchange contribution $\sigma^{-}d\sigma/dt(K^{-}n \to \bar{K}^{*0}\Delta^{0})$(●), compared to $\sigma^{-}d\sigma/dt$ $(K^{*0}\Delta^{++})$ (○).

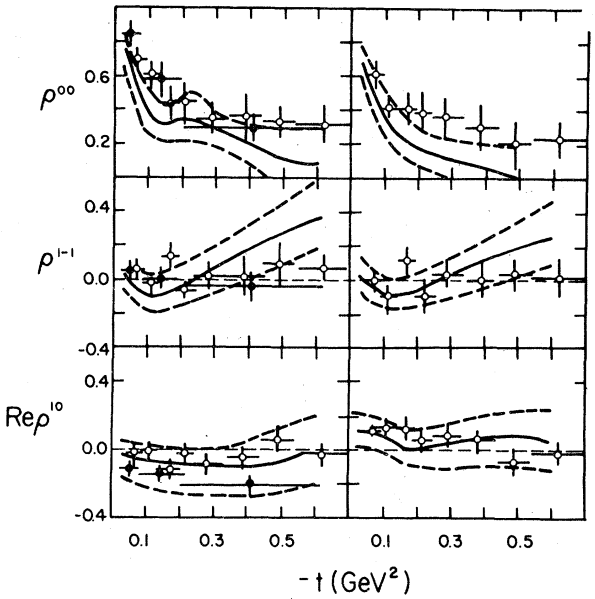

FIG. 29. Comparison of the SU(3)-predicted (solid curve) and experimentally determined density matrix elements for the reaction $K^{-}n \to \bar{K}^{*0}\Delta^{-}$ at 5.5 GeV/c (○) and $K^{-}p \to \bar{K}^{*0}\Delta^{0}$ at 10 GeV/c (●) in Gottfried-Jackson and helicity frames. The dashed bands correspond to an estimate of the errors of the SU(3) predictions as deduced from the errors due to interpolation of the quoted data for $K^{+}p \to K^{*0}\Delta^{++}$, $\pi^{+}p \to \rho^{0}\Delta^{++}$, and $\pi^{+}p \to \omega\Delta^{++}$.

but is contrary to what is observed in many other line-reversal-related processes, where the cross section of the "real" reaction is found to be larger than that of the rotating reaction.

The results (38) and (39) imply that

$$\sigma^{1-}d\sigma/dt(K^{*0}\Delta^{++}) \simeq \sigma^{1-}d\sigma/dt(\bar{K}^{*0}\Delta^{-}) \qquad (40)$$

in both frames. In the conventional absorption model for π and B exchanges, $\sigma^{1-}d\sigma/dt$ in the Gottfried-Jackson frame cannot receive contributions from the poles themselves. Instead, contributions result only from their cut correction terms, so that (40) places a rather stringent constraint on the relative phases of the Regge cuts.

In Fig. 29, we use the extrapolated data for $\pi^{+}p \to \rho^{0}\Delta^{++}$, $\pi^{+}p \to \omega\Delta^{++}$, and $K^{+}p \to K^{*0}\Delta^{++}$ to predict the density matrix elements ρ^{00}, ρ^{11}, and Re ρ^{10} for $K^{-}n \to \bar{K}^{*0}\Delta^{-}$ and $K^{-}p \to \bar{K}^{*0}\Delta^{0}$.

These predictions (solid curve) are compared with the $K^{-}n \to \bar{K}^{*0}\Delta^{-}$ data at 5.5 GeV/c (Ref. 30) (open circles) and $K^{-}p \to \bar{K}^{*0}\Delta^{0}$ data at 10 GeV/c (Ref. 29) (closed circles). The dashed bands correspond to an estimate of the errors of the prediction as deduced from the errors of the extrapolations of the quoted data on $K^{+}p \to K^{*0}\Delta^{++}$, $\pi^{+}p \to \rho^{0}\Delta^{++}$, and $\pi^{+}p \to \omega\Delta^{++}$. We observe that the predicted values deduced using SU(3) sum rule (35) are in excellent agreement with the reported data.

In conclusion, it appears that even in the presence of cut contributions, the existing $d\sigma/dt$ and vector-meson density matrix elements for the processes $\pi^{+}p \to \rho^{0}\Delta^{++}$, $\pi^{+}p \to \omega\Delta^{++}$, $K^{+}p \to K^{*0}\Delta^{++}$, $K^{-}n \to \bar{K}^{*0}\Delta^{-}$, and $K^{-}p \to \bar{K}^{*0}\Delta^{0}$ are consistent with SU(3) symmetry, i.e., that these processes are dominated by the same two sets of SU(3) octet exchanges ($G=+1$ and $G=-1$).

XII. QUARK ADDITIVITY

Białas and Zalewski[31] obtained constraints on the single and joint decay matrix element in double resonance reactions using the nonrelativistic quark model. Their predictions may be divided into three classes A, B, and C, differentiated by an increasing severity of theoretical assumptions. The "class A" relations depend only on the additivity assumption that the full scattering amplitude is a coherent sum of single quark-quark scattering subinteractions, and that parity is conserved for

TABLE X. Białas and Zalewski quark-model relationships in transversity frames.

Class A	A.1	$T_{00}^{20} = \sqrt{2}\, T_{00}^{02}$
	A.2	$\mathrm{Re}T_{20}^{22} = \frac{1}{2}\mathrm{Re}T_{20}^{20}$
	A.3	$\mathrm{Re}T_{02}^{22} = \frac{1}{\sqrt{2}}\mathrm{Re}T_{02}^{02}$
	A.4	$T_{00}^{22} = \frac{1}{2\sqrt{6}} - \frac{1}{\sqrt{2}} T_{00}^{02}$
	A.5	$\mathrm{Im}T_{20}^{22} = \frac{1}{2}\mathrm{Im}T_{20}^{20}$
	A.6	$\mathrm{Im}T_{02}^{22} = \frac{1}{\sqrt{2}}\mathrm{Im}T_{02}^{02}$
Class B	B.1	$\mathrm{Re}T_{20}^{20} = \sqrt{2}\,\mathrm{Re}T_{02}^{02}$
	B.2	$\mathrm{Im}T_{20}^{20} = \sqrt{2}\,\mathrm{Im}T_{02}^{02}$
	B.3	$\mathrm{Re}T_{20}^{22} = \mathrm{Re}T_{02}^{22}$
	B.4	$\mathrm{Im}T_{20}^{22} = \mathrm{Im}T_{02}^{22}$
	B.5	$\mathrm{Im}T_{2-2}^{22} = 0$
	B.6	$\mathrm{Im}T_{1-1}^{22} = 0$
Class C	C.1	$\mathrm{Im}T_{02}^{02} = 0$
	C.2	$\mathrm{Im}T_{20}^{20} = 0$
	C.3	$\mathrm{Im}T_{22}^{22} = 0$
	C.4	$\mathrm{Im}T_{20}^{22} = 0$
	C.5	$\mathrm{Im}T_{11}^{22} = 0$
	C.6	$\mathrm{Im}T_{02}^{22} = 0$
	C.7	$\frac{1}{\sqrt{6}} - (T_{22}^{22} + T_{2-2}^{22} + T_{00}^{22}) = 0$

each quark-quark scattering process. These class A relations are invariant under arbitrary independent rotations of either the vector meson or the Δ^{++} coordinate system about the production plane normal. By invoking time-reversal and charge-conjugation invariance for free quark-quark scattering, one can obtain the class B and class C relations. The class B relations are invariant under arbitrary equal rotations of the vector meson and the Δ^{++} coordinate systems about the normal, while class C relations have no such simple rotational properties, and are thus expected to be valid in one and only one coordinate system.

It has been noted by Białas and Zalewski[31] that a strict interpretation in terms of free-quark scattering leads to results at the particle level which depend on the reference frame in which the calculation is performed. Thus these authors were led to consider classes B and C as independent sets of relations which may hold in only definite reference frames. In a relativistic treatment of quark-quark scattering Lipkin[32] has shown that neither class B nor class C should be expected to be valid, so that searches for suitable frames become pointless.

However, assuming dipole interactions at the baryon vertex in the t channel, class A and class B relations can be directly deduced, while class C relations cannot.[33] The derivation of the dipole model (DM) suggests that class A and class B relations are expected to be valid in the t-channel coordinate system (Gottfried-Jackson frame), but may be only approximately satisfied in the s-channel (helicity frame).

These quark-model relationships take on their simplest form when expressed in terms of statistical tensors[34] in transversity frames, as presented in Table X.

In Figs. 30 and 31, we show, as a function of $-t$, the left and right sides respectively of the class A and B relations for reaction (1) in both frames. For reaction (2) all but four of the 12 relations are satisfied to within one standard deviation. Of these four, three are satisfied to this level in the Gottfried-Jackson frame and to within two standard deviations in the helicity frame. The

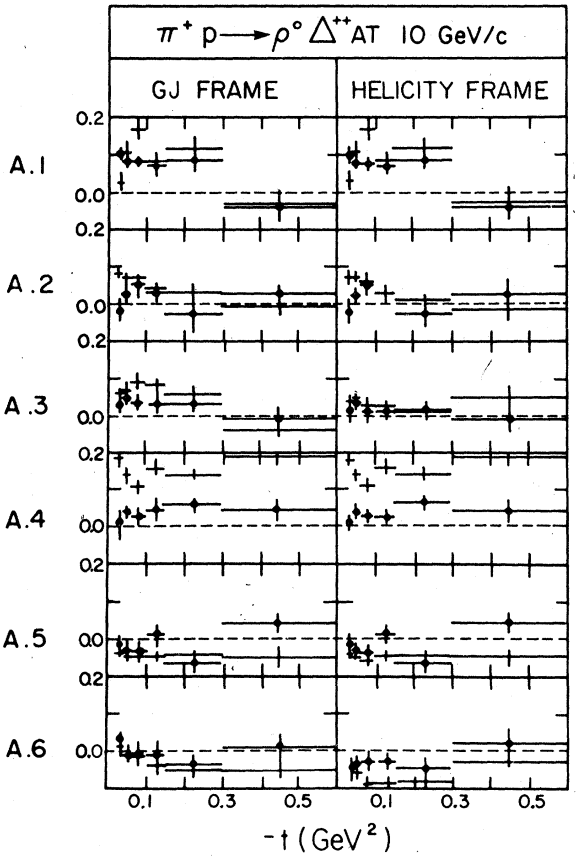

FIG. 30. Comparison of the quark-model class A predictions with $\rho^0\Delta^{++}$ data in the transverse Gottfried-Jackson and helicity frames.

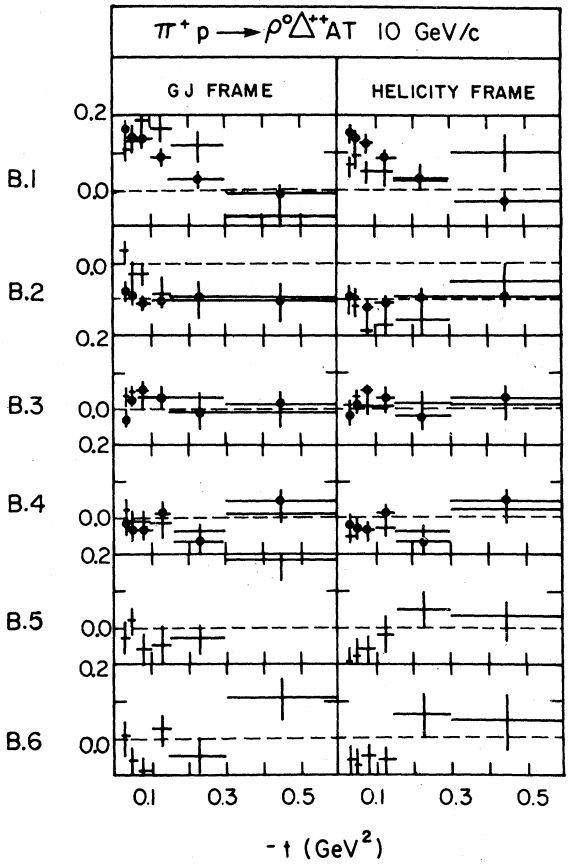

FIG. 31. Comparison of the quark-model class B predictions with $\rho^0\Delta^{++}$ data in the transverse Gottfried-Jackson and helicity frames.

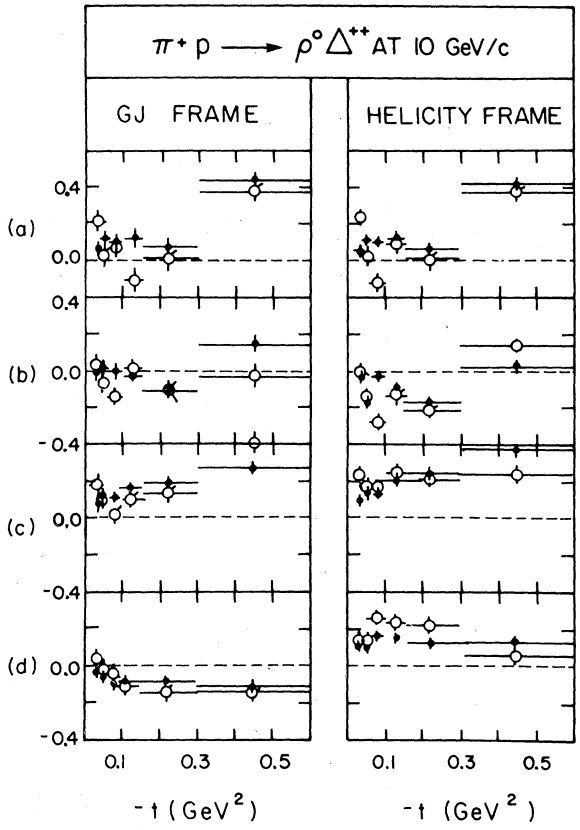

FIG. 32. Comparison of right- (●) and left- (○) hand sides of Eqs. (41) for the $\rho^0\Delta^{++}$ channel.

remaining relation, A.4, yields a difference between the left and right sides of 0.18 ± 0.04 in both frames.

It may be seen that the overall agreement of the data with these relations is quite satisfactory for both reactions. The most important deviations are observed in the A.4 relations, which implies the following equality:

$$f_{1(1/2)(-1/2)} = f_{1(3/2)(1/2)}/\sqrt{3} \ .$$

Results for class C relations (not shown) are not found to be simultaneously satisifed in any reference frame for either $\rho^0\Delta^{++}$ and $\omega\Delta^{++}$.

When rotated into the usual (nontransverse) Gottfried-Jackson or helicity frame, the first class A prediction, (A.1), specifies a relation between single vertex density matrix elements:

$$\rho^{11} + \rho^{1-1} = \tfrac{4}{3}\rho_{33} + \left(\frac{4}{\sqrt{3}}\right)\rho_{3-1} \ . \tag{41a}$$

If the class B prediction is also assumed, the following three equalities result[34]:

$$\rho^{11} = \tfrac{4}{3}\ \rho_{33} \ , \tag{41b}$$

$$\rho^{1-1} = \left(\frac{4}{\sqrt{3}}\right)\rho_{3-1} \ , \tag{41c}$$

$$\rho^{10} = \left(\frac{4}{\sqrt{6}}\right)\rho_{31} \ . \tag{41d}$$

Both the left and right sides of these relations are plotted for $\rho\Delta$ ($\omega\Delta$) data in Fig. 32 (Fig. 33). All these conditions are reasonably well satisfied. However, the class C conditions $\rho^{10} = 0$ and $\rho_{31} = 0$ are clearly invalid.

Similar conclusions have been reported at 3.7 GeV/c,[35] 5.0 GeV/c,[36] 8.0 GeV/c,[37] 13.1 GeV/c,[1v], and 16 GeV/c.[2t]

We have shown that the quark-additivity assumptions (classes A and B) are generally well satisfied. It should be noted, however, that any model with cut contributions in the zero-helicity-flip amplitudes must approximately satisfy these quark-model constraints.

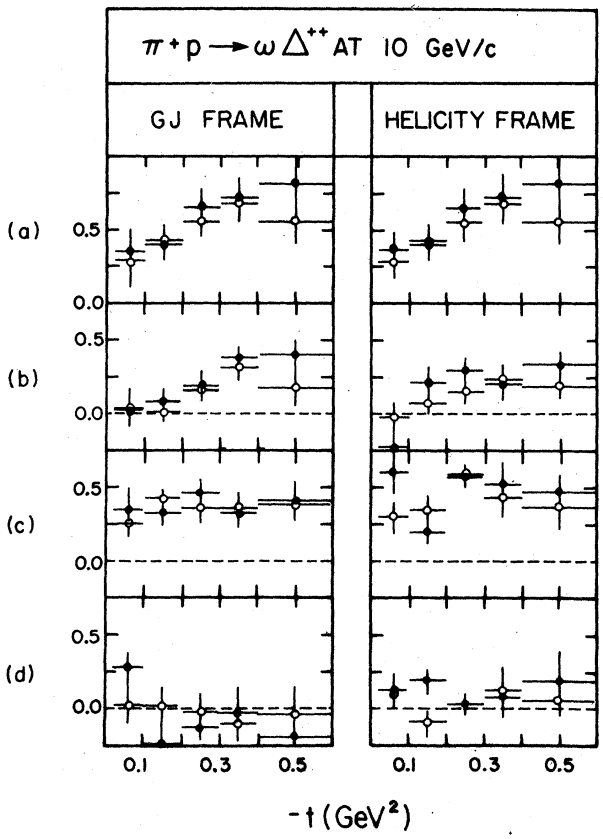

FIG. 33. Comparison of right- (●) and left- (○) hand sides of Eqs. (41) for the $\omega\Delta^{++}$ channel.

XIII. AMPLITUDE ANALYSIS OF THE REACTION $\pi^+ p \to \rho^0 \Delta^{++}$

The basic goal of model construction for high-energy two-body and quasi-two-body reactions is to understand the structure of the underlying amplitudes. Therefore, the extraction of the amplitudes from the data is of prime importance.

However, in the reaction $\pi^+ p \to \rho^0 \Delta^{++}(1236)$, the number of observables is insufficient for a complete amplitude determination, thereby necessitating certain model-dependent assumptions. The method used here, due to Irving,[38] makes several assumptions which sufficiently reduce the number of independent amplitudes so that the remaining terms may be extracted from the data. The interest of such an approach lies in its application to a large number of reactions and in the search for regular simple features in the model dependent amplitudes thus obtained.

A. The method

The results of the analysis are most easily interpreted if they are presented in terms of s-channel helicity amplitude combinations which receive contributions from t-channel exchanges of definite naturality. The appropriate natural- and unnatural-parity-exchange amplitudes, $N^{\lambda}_{2\lambda_\Delta \lambda_\rho}$ and $U^{\lambda_\rho}_{2\lambda_\Delta \lambda_p}$, labeled by the helicities of the ρ, Δ, and proton, λ_ρ, λ_Δ, and λ_p, respectively, are defined in terms of helicity amplitudes $H^{\lambda_\rho}_{2\lambda_\Delta \lambda_p}$. Each of these latter amplitudes is characterized by a value of $n = |\lambda_p - \lambda_\Delta + \lambda_\rho|$.

Imposing a set of rather general assumptions and taking into account the presence of the S-wave $\pi\pi$ system, the method proposed in Ref. 38 allows the extraction of six P-wave U and N amplitudes. For each $-t$ value, we determined those parameters from our data by a χ^2 fit to the 30 available moments. In each case, the overall phase was fixed by requiring that U^0_{3+} be real and positive. In Fig. 34, the moduli of the s-channel amplitudes and their relative phases are presented.

B. Discussion

Although the statistical significance of our data is poor, a brief discussion of the gross features of the amplitudes can be made.

(a) The two $n=1$ amplitudes, U^0_{3+} and U^1_{1+}, are expected to be dominated by π exchange; therefore their relative phase is expected to be zero, in agreement with the results of the model-dependent analysis.

(b) U^0_{1+} has $n=0$ and should be dominated by π exchange with the possible presence of additional cut terms. The magnitude of U^0_{1+} shows the steep falloff at small $-t$ expected from π exchange. However, the phase of U^0_{1+} is substantially different from zero, which is evidence for a cut contribution.

(c) U^1_{3+} is a combination of $n=0$ and $n=2$ helicity amplitudes. The results indicate structure in both the magnitude and the phase. The magnitude shows a dip at $-t \simeq 0.06$ GeV^2, whereas the phase abruptly shifts from near 180° to near 0° at this same $-t$ value. This type of structure is characteristic of pole-cut interference and has been seen in $\pi^- p \to \rho^0 n$ at 17.2 GeV/c (Ref. 16) and $\pi^+ p \to \rho^0 \Delta^{++}(1236)$ at 7.1 GeV/c.[39]

(d) The natural-parity exchange amplitude N^1_{3+} is a combination of $n=0$ and $n=2$ helicity amplitudes and, as such, should show the characteristic pole-cut interference structure discussed above. indeed, the magnitude of N^1_{3+} is observed to have a change of slope at $-t \simeq 0.2$ GeV^2, but no strong structure is seen in its phase.

(e) The amplitude N^1_{1+} (predicted to be zero in the quark model) is small and the errors on both magnitude and phase are large.

These results are in agreement with the findings

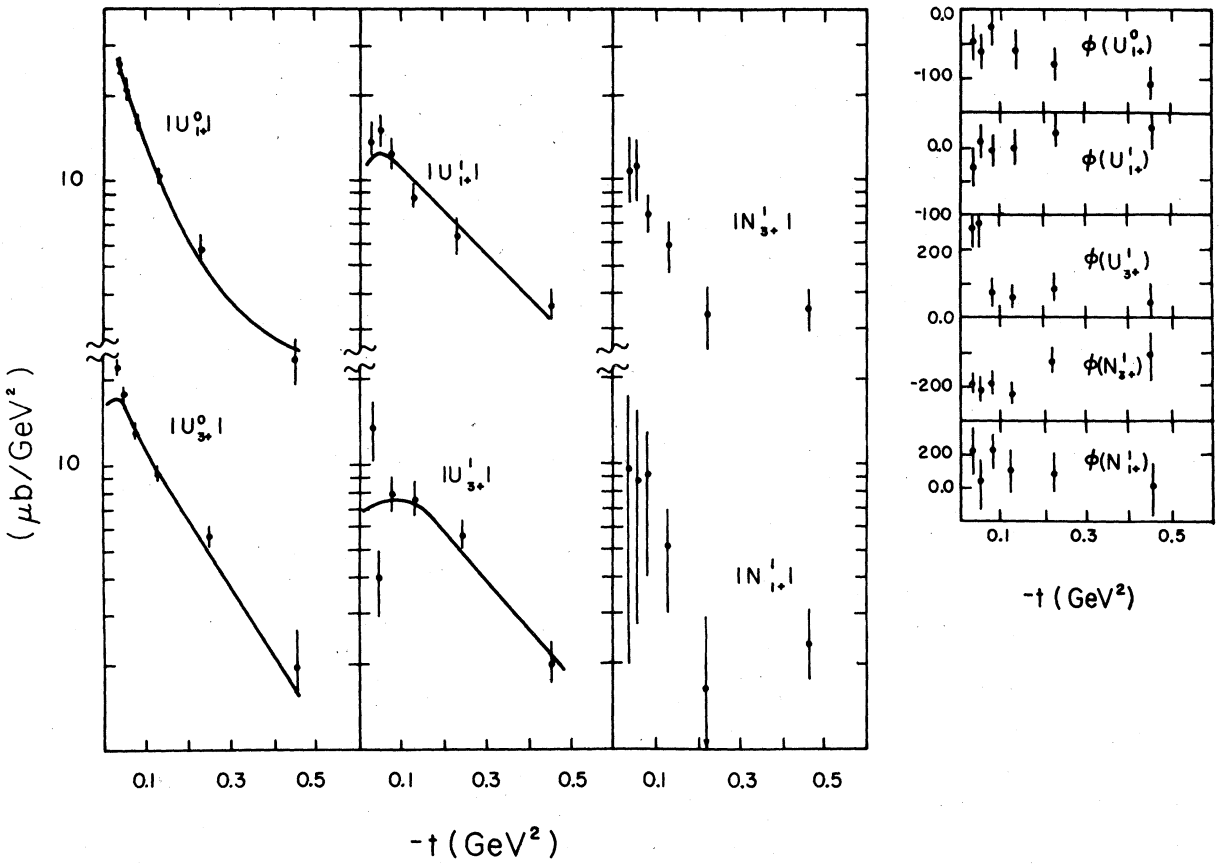

FIG. 34. Magnitudes and phases of the unnatural- (U) and natural- (N) parity-exchange amplitudes for the reaction $\pi^+ p \to \rho^0 \Delta^{++}$. The curves are described in the text. The amplitudes are normalized to the differential cross section.

of the amplitude analysis performed with the same model-dependent assumptions at 7.1 GeV/c.[39]

It has been suggested that the phenomenology of two-body reactions, which is apparently rather complicated in terms of t-channel exchange, may look very simple when viewed in terms of s-channel dyanmics.[40] For instance, if one considers the impact-parameter profile of each s-channel helicity amplitude with net helicity flip n, it has been postulated that there exists a "universal impact parameter" criterion or "b universality" which trivially relates these profiles for different values of n.[40] It is interesting to note that the additive quark model also suggests[22] that the helicity amplitudes depend only on n.

To describe π-exchange reactions, Humble[41] proposed a modification to the "b-universality" hypothesis which gives an excellent quantitative fit to the $\pi^- p \to \rho^0 n$ and $\pi^- p \to fn$ data.

The results of the application of this model to our data for reaction (1) are shown by the solid curves in Fig. 34: $|U^0_{1+}|$, $|U^0_{3+}|$, and $|U^1_{1+}|$ are found to be well described by Humble's parametrization. However, our statistics are insufficient to reproduce the low $-t$ dip in $|U^1_{3+}|$, predicted by the model.[41] Similarly, one is tempted to conclude that the structure observed in N^1_{3+} might be due to a combination of the Bessel function $|J_0|^2$ and $|J_2|^2$ as predicted by the dual absorptive model[42] with $|J_0|^2$ dominating, and no substantial real part.[16]

From this model-dependent amplitude analysis, we conclude that our data are compatible with a simple interpretation in terms of geometrical-optical ideas[40] and suggest a generalized factorization of the type[22]

$$f_{\{\lambda_i\}} = \gamma_{\lambda_a \lambda_c}\, \gamma_{\lambda_b \lambda_d}\, \bar{f}_n(s,t)\,,$$

where $\bar{f}_n(s,t)$ would depend on the total helicity transfer n and would be equal for all reactions participating in an SU(3) relation.

XIV. CONCLUSIONS

A systematic analysis of the reactions $\pi^+ p \to (\rho^0, \omega)\Delta^{++}(1236)$ yielded cross sections, dif-

ferential cross sections, and vector-meson and $\Delta^{++}(1236)$ single and joint decay spin-density matrix elements.

From these results we conclude that the reaction $\pi^+ p \to \rho^0 \Delta^{++}(1236)$ is dominated, in the small-momentum-transfer region, by unnatural parity exchange (presumably π exchange) contributing to net-helicity-zero amplitudes. However, we have noted that additional cut contributions, mainly associated with $n=0$ amplitudes, are necessary to describe the data. At larger $-t$ values, the natural-parity-exchange contribution (e.g., A_2 exchange) becomes important, but this contribution also needs cut corrections. In $\pi^+ p \to \omega\Delta^{++}$ (1236), natural- and unnatural-parity exchanges contribute significantly over the whole $-t$ region. Cut contributions are also present in this reaction.

It appears that these cut contributions, i.e., the nonpole-like part of the amplitudes, seem to have properties in common with Regge poles. Indeed, we found that their presence does not strongly affect the validity of SU(3) factorization or the quark-additivity predictions, and that their main effects seem to be concentrated in the modification of the Regge-pole phase.

Finally, we demonstrated the possibility of describing the amplitudes in terms of s-channel dynamics with a simple factorization property.

ACKNOWLEDGMENTS

This experiment could not have taken place without the participation of a large number of people. We want especially to thank those physicists who took part in the early stages of the experiment and made important contributions to its progress: Gordon Charlton, Dave Crennell, Brian Deery, Dave Gilbert, Howard Gordon, K. W. Lai, George Luste, Suzanne Vallet, and Taek-Soon Yoon. Equally important was the work of measuring, scanning, programming, and data handling. In particular, we want to thank the following who contributed so much in these areas: Quais Ashraf, Bruce Bolin, Rodney Jones, Peter Kahan, Dave Kesterton, June Liu, Shelia Maggs, Dave McDonald, John Phillips, Alfred Sipprell, and the large band of measurers and scanners at Toronto.

We also express our appreciation to the POLLY group and all members of the SLAC staff who contributed to the success of the data acquisition.

This work was supported by funds from the National Research Council of Canada, administered by the Institute of Particle Physics.

---

*Present address: Department of Physics, Purdue University, Lafayette, Indiana 47907.

†Present address: Argonne National Lab., 9700 So. Cass Ave., Illinois 60439.

[1](a) 2.08 GeV/c: F. E. James *et al.*, Phys. Rev. 142, 896 (1966); (b) 2.34 GeV/c: N. Angelov *et al.*, Dubna Report No. JINRP P1-4611, 1969 (unpublished); (c) 2.35, 2.62, and 2.9 GeV/c: C. Alff-Steinberger *et al.*, Phys. Rev. 145, 1072 (1966); (d) 2.77 GeV/c: S. S. Yamamoto *et al.*, Phys. Rev. 140, B730 (1965); (e) 2.95, 3.19, 3.53, 3.74, and 4.08 GeV/c: D. Brown *et al.*, Phys. Rev. D 1, 3053 (1970); (f) 3.43 and 3.54 GeV/c: M. Abolins *et al.*, Phys. Rev. Lett. 11, 381 (1963); (g) 3.5 GeV/c: E. E. Ronat *et al.*, Nucl. Phys. B38, 20 (1972); (h) 3.65 GeV/c: G. H. Trilling *et al.*, Phys. Lett. 19, 427 (1965); (i) 3.7 GeV/c: G. S. Abrams *et al.*, Phys. Rev. Lett. 25, 617 (1970); (j) 3.9 GeV/c: B. Haber *et al.*, Phys. Rev. D 11, 495 (1975); (k) 4.0 GeV/c: M. Aderholz *et al.*, Nuovo Cimento 35, 659 (1965); (l) 4.93 GeV/c: Y. Eisenberg *et al.*, Phys. Lett. 48B, 354 (1974); (m) 5.0 GeV/c: C. L. Pols *et al.*, Nucl. Phys. B25, 109 (1970); (n) 5.1 GeV/c: N. Armenise *et al.*, Nuovo Cimento 65A, 637 (1970); (o) 5.45 GeV/c: I. J. Bloodworth *et al.*, Nucl. Phys. B35, 79 (1971); (p) 5.72 GeV/c: A. Sheng, MIT thesis (unpublished); (q) 7.04 GeV/c: P. Slattery *et al.*, Nuovo Cimento 50, 377 (1967); (r) 7.1 GeV/c: S. U. Chung *et al.*, Phys. Rev. D 12, 693 (1975); (s) 8.04 GeV/c: M. Aderholz *et al.*, Nucl. Phys. B8, 45 (1968); (t) 8.49 GeV/c: H. H. Kung, Columbia University thesis, 1970 (unpublished); (u) 11.7 GeV/c: R. O. Maddock *et al.*, Nuovo Cimento 5A, 433 (1971); (v) 13.1 GeV/c: J. A. Gaidos *et al.*, Nucl. Phys. B72, 253 (1974); (w) 16.0 GeV/c: R. Honecker *et al.*, Nucl. Phys. B106, 365 (1976); (x) 18.5 GeV/c: N. N. Biswas *et al.*, Phys. Rev. D 2, 2529 (1970).

[2](a) 2.3 and 2.67 GeV/c: W. Ko *et al.*, UCRL Report No. 19779, 1970 (unpublished); (b) 2.34 GeV/c: N. Angelov *et al.*, Dubna Report No. JINRP P1-4611, 1969 (unpublished); (c) 2.75 GeV/c: N. Armenise *et al.*, Nuovo Cimento 40A, 273 (1965); (d) 2.77 GeV/c: S. S. Yamamoto *et al.*, Phys. Rev. 140, B730 (1965); (e) 2.95, 3.19, 3.53, 3.74, and 4.08 GeV/c: D. Brown *et al.*, Phys. Rev. D 1, 3053 (1970); (f) 3.5 GeV/c: E. E. Ronat *et al.*, Nucl. Phys. B38, 20 (1972); (g) 3.65 GeV/c: G. H. Trilling *et al.*, Phys. Lett. 19, 427 (1965); (h) 3.7 GeV/c: G. S. Abrams *et al.*, Phys. Rev. Lett. 25, 617 (1970); (i) 4.0 GeV/c: M. Aderholz *et al.*, Phys. Rev. D 9, 3015 (1974); (j) 4.09 GeV/c: D. G. Fong *et al.*, Phys. Rev. D 9, 3015 (1974); (k) 5.0 GeV/c: C. L. Pols *et al.*, Nucl. Phys. B25, 109 (1969); (l) 5.45 GeV/c: I. J. Bloodworth *et al.*, Nucl. Phys. B35, 79 (1971); (m) 5.72 GeV/c: A. Sheng, MIT thesis (unpublished); (n) 7.0 GeV/c: P. Slattery *et al.*, Nuovo Cimento 50, 377 (1967); (o) 7.1 GeV/c: S. U. Chung *et al.*, Phys. Rev. D 12, 693 (1975); (p) 8.04 GeV/c: M. Aderholz *et al.*, Nucl. Phys. B8, 45 (1968); (q) 8.49 GeV/c: H. H. Kung, Columbia University thesis, 1970 (unpublished); (r) 11.7 GeV/c: D. Evans *et al.*, Nucl. Phys. B51, 205 (1973); (s) 13.1 GeV/c: J. A.

Gaidos *et al.*, Nucl. Phys. B72, 253 (1974); (t) 16 GeV/c: H. Grassler *et al.*, Nucl. Phys. B115, 365 (1976); (u) 18.5 GeV/c: N. N. Biswas *et al.*, Phys. Rev. D 2, 2529 (1970).
[3]C. N. Kennedy *et al.*, Phys. Rev. D 17, 2888 (1978); C. N. Kennedy, Ph.D. thesis, University of Toronto, 1976 (unpublished).
[4]M. Aguilar-Benitez *et al.*, Phys. Rev. D 6, 29 (1972).
[5]D. G. Coyne *et al.*, Nucl. Phys. B32, 333 (1971).
[6]G. Wolf, Phys. Rev. Lett. 19, 925 (1967).
[7]W. Lohmann and H. J. Schreiber, Berlin Report No. PHE 75-11, 1975 (unpublished).
[8]M. Aguilar-Benitez, S. U. Chung, and R. L. Eisner, Phys. Rev. D 6, 11 (1972).
[9]J. Daboul, Nucl. Phys. B4, 180 (1967).
[10]H. Pilkuhn and B. E. Y. Svensson, Nuovo Cimento 38, 518 (1965).
[11]J. T. Donohue, Nuovo Cimento 52A, 1152 (1967).
[12]J. T. Donohue *et al.*, Nucl. Phys. B117, 173 (1976).
[13]J. P. Ader *et al.*, Nuovo Cimento 56A, 952 (1968).
[14]K. Shiga, Kyushu Sangyo University, Report No. KSU-102, 1973 (unpublished).
[15]See, for instance, J. F. Owens *et al.*, Nucl. Phys. B94, 77 (1975).
[16]P. Estabrooks and A. D. Martin, Phys. Lett. 41B, 350 (1972).
[17]G. Ciapetti *et al.*, Nucl. Phys. B64, 58 (1973).
[18]P. K. Williams, Phys. Rev. D 1, 1312 (1970).
[19]M. G. Doncel *et al.*, Phys. Rev. D 7, 815 (1973).
[20]A. Kotanski and K. Zalewski, Nucl. Phys. B4, 559 (1968).
[21]J. T. Donohue and G. Plaut, Phys. Lett. 41B, 495 (1972); F. Schrempp and B. Schrempp, in *High Energy Physics*, proceedings of the European Physical Society International Conference, Palermo, 1975, edited by A. Zichichi (Editrice Compositori, Bologna, 1976), p. 682.
[23]M. A. Wahlig and I. Mannelli, Phys. Rev. 168, 1515 (1968).
[24]D. W. G. Leith, in *Proceedings of the Conference on Phenomenology in Particle Physics, 1971* (Caltech, Pasadena, Calif., 1971), p. 554.
[25]E. Bracci *et al.*, Report No. CERN-HERA 72-1, 1972 (unpublished).
[26]J. D. Dowell *et al.*, Nucl. Phys. B108, 30 (1976).
[27]M. Le Bellac, Phys. Lett. 25B, 524 (1967).
[28]G. Ciapetti *et al.*, Nucl. Phys. B66, 350 (1973).
[29]M. Deutschmann *et al.*, Nucl. Phys. B36, 373 (1972).
[30]B. Wener *et al.*, Nucl. Phys. B23, 37 (1970).
[31]A. Bialas and K. Zalewski, Nucl. Phys. B6, 465 (1968).
[32]H. J. Lipkin, Nucl. Phys. B20, 652 (1970).
[33]L. Jones, Phys. Rev. 163, 1530 (1967). G. S. Abrams, K. W. J. Barnham, and J. J. Bosognana, Phys. Rev. D 8, 1435 (1973).
[34]A. Kotanski and K. Zalewski, Nucl. Phys. B13, 119 (1969).
[35]G. S. Abrams and K. W. J. Barnham, Phys. Rev. D 7, 1395 (1973).
[36]L. Lyons *et al.*, Nucl. Phys. B85, 165 (1975).
[37]M. Aderholz *et al.*, Nucl. Phys. B8, 485 (1968).
[38]A. C. Irving, Nucl. Phys. B63, 499 (1973).
[39]J. F. Owens *et al.*, Nucl. Phys. B112, 514 (1976).
[40]B. Schrempp and F. Schrempp, Nucl. Phys. B54, 525; (1973); S. Humble, *ibid.* B76, 137 (1974); J. P. de Brion and R. Peschanski, *ibid.* B81, 484 (1974); J. P. Ader *et al.*, Nuovo Cimento 27A, 385 (1975).
[41]S. Humble, Nucl. Phys. B98, 267 (1975).
[42]H. Harari, Ann. Phys. (N.Y.) 63, 432 (1971); Phys. Rev. Lett. 26, 1400 (1971).